Pseudo-Gapped State in CeNiSn

Koichi IZAWA

Department of Physics, Faculty of Science,
Hiroshima University
1-3-1 Kagamiyama, Higashi-Hiroshima 739, Japan

February, 1998

Abstract

Thermal and magnetic properties of CeNiSn have been measured on a high-quality single crystal in magnetic fields in order to reveal the intrinsic ground state of this compound. The specific heat for the purified crystal has been found to remarkably depend on the field along the a axis in contrast with less field dependence for dirty samples. The electronic specific heat divided by temperature C_{el}/T increases around 2 K with increasing field along the a axis, indicating that the field enhances the density of states (DOS) around Fermi level $E_{\rm F}$ in this temperature range. On the other hand, C_{el}/T around 7 K decreases with increasing field. To understand the origin of temperature and field dependence of C_{el}/T, we introduced a DOS model which consists of a V-shaped gap with a residual DOS in the Lorentzian peak around $E_{\rm F}$. The experimental result is well reproduced by assuming the Zeeman splitting of the DOS without changing the shape of the gap by magnetic field. This result indicates that the gap above 2 K is hardly affected by applying field at least up to 14 T.

The C_{el}/T below 2 K stays nearly constant in zero field. With further decreasing temperature, C_{el}/T slightly increases below 0.5 K, which suggests that there is a peak structure at the bottom of the pseudo-gap around $E_{\rm F}$. However, the large reduction of C_{el}/T in the field has been found, suggesting that a rigid band picture is no more realistic below 1 K. The field dependence indicates that the peak inside the pseudo-gap is collapsed by external field. In this study, we concluded that CeNiSn is classified as a new-type Kondo metal instead of a Kondo insulator.

Contents

List of Figures

List of Tables

Chapter 1

Introduction

1.1 Ce-based compounds

Since the discovery of "heavy fermion" phenomena [1] in Lanthanide and Actinide compounds, a considerable number of active studies has been made on these compounds. In particular, Ce-based compounds show a variety of unusual ground states due to the peculiar character of the $4f$ electron, including a non-magnetic heavy-fermion state, a magnetic ordering state and a superconducting state [2, 3, 4].

The electron configuration in a Ce atom is

$$\mathrm{Ce} : [\mathrm{Xe}]4f^1 5s^2 5p^6 5d^1 6s^2.$$

In many cases, a Ce ion has a trivalent state (Ce^{3+}) in a compound. The $5d^1 6s^2$ electrons are to be conduction electrons. The $4f$ electron is located inside the $5s5p$ shells and well localized at high temperatures. With decreasing temperature, a spin-flip scattering (Kondo scattering) of conduction electrons becomes dominant at each Ce site similar to the well-established dilute-Kondo effect. In this temperature region, electric resistivity ρ shows logarithmic temperature dependence and magnetic susceptibility χ exhibits the Curie-Weiss temperature dependence. As temperature is further decreased below a characteristic temperature T_{K} (Kondo temperature), the resistivity marks a maximum and a rapid decrease follows. At lower temperatures, ρ is proportional to T^2. The magnetic

susceptibility deviates from the Curie-Weiss law and tends to level off due to the realization of the enhanced Pauli paramagnetism with $\sim 10^{-3}$ emu/mol below T_K. In this temperature range, the ratio of electronic specific heat to temperature C_{el}/T remarkably increases up to a constant value of $100 \sim 1000$ mJ/K^{2}mol in contrast with a few mJ/K^{2}mol for a usual metal. The behavior below T_K originates from the formation of a narrow quasiparticle band around Fermi level E_F due to the conduction and f electron (c-f) hybridization. The quasiparticle state is well described as a Fermi liquid state. As the quasiparticle band has flat dispersion, a peak is developed in the density of states (DOS) around E_F. The peak is called as the Kondo peak or the Abrikosov-Shul resonance peak. The phenomena mentioned above are referred to as the dense-Kondo effect. The large values of C_{el}/T and χ are ascribed to a large effective mass of quasiparticles. Therefore, such dense-Kondo compounds are frequently called as "heavy fermion system".

The quasiparticles form various ground states; a heavy-fermion state, an unusual magnetic orders, a superconducting state and a (pseudo-) energy gapped state. The energy gap formation has been suggested in CeNiSn [5, 6, 7, 8], $Ce_3Bi_4Pt_3$ [9] and CeRhSb [10] SmB_6 [11], YbB_{12} [12] and so on.

1.2 CeNiSn

CeNiSn crystallizes in an ϵ-TiNiSi type orthorhombic structure [13, 14] as illustrated in Fig. 1.1. The lattice parameters are $a = 7.542(1)$ Å, $b = 4.6009(4)$ Å and $c = 7.617(1)$ Å at room temperature. A Ce atom is surrounded by a pair of two distorted hexagonal rings which are linked by Ni and Sn atoms alternatively, and the Ce atoms form a zig-zag chain along the a axis. Although the exact Ce-site symmetry is monoclinic (Cs), the symmetry is frequently treated as pseudo-trigonal because the distortion of the hexagonal Ni-Sn ring is small.

Magnetic susceptibility does not follow the Curie-Weiss law below 300 K. A

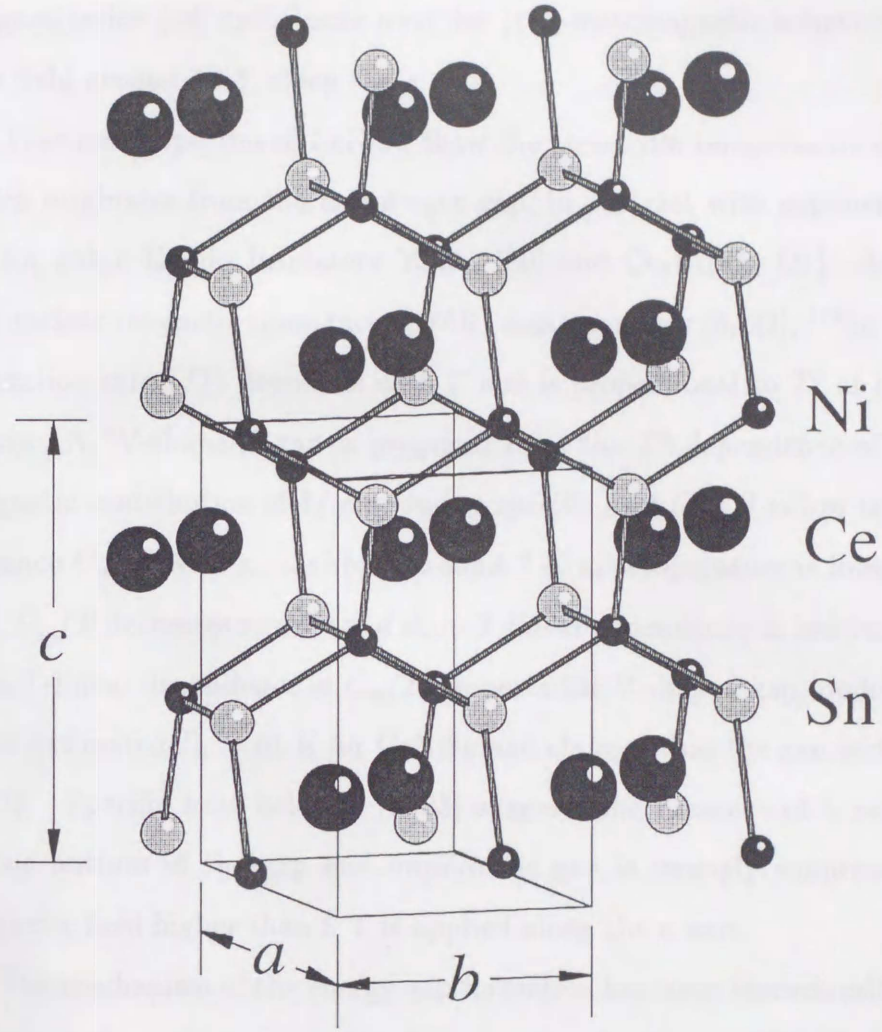

Figure 1.1: Crystal structure of CeNiSn.

peak structure was observed around 12 K in the magnetic susceptibility along the a axis, which is the easy magnetization axis. Before the present study, the peak was believed to reflect development of antiferromagnetic correlation suggested by inelastic neutron scattering experiments [15]. Because of high T_K, well-defined peak corresponding to crystal-field excitation was not found in inelastic neutron scattering [16], although a broad peak was indistinctly detected at 4.2 K [17]. In

magnetization [18] and elastic modulus [19], metamagnetic behavior was found in a field around 10 T along the a axis.

Thermal properties of CeNiSn show the power law temperature dependence, which originates from the anisotropic gap, in contrast with exponential behavior for cubic Kondo Insulators YbB_{12} [20] and $Ce_3Bi_4Pt_3$ [21]. According to the nuclear magnetic resonance (NMR) measurements [6, 22], ^{119}Sn spin-lattice relaxation rate $1/T_1$ decreases with T and is proportional to T^3 at low temperatures. A "V-shaped" gap is proposed from the T^3 dependence of $1/T_1$. The magnetic contribution of $4f$ electron to specific heat C_m [7] at low temperatures enhance C_m/T with a maximum around 7 K as temperature is lowered. Below 7 K, C_m/T decreases rapidly and show T-linear dependence at low temperatures. This T-linear dependence of C_m/T supports the V-shaped gap model. Nishigori *et al.* estimated $T_K = 51$ K for CeNiSn and claimed that the gap width is scaled by T_K. Specific heat below 1 K [23] suggests the presence of a residual DOS at the bottom of the gap and implies the gap is strongly suppressed when a magnetic field higher than 8 T is applied along the a axis.

The mechanism of the energy gap formation has been theoretically discussed from a various view points [24, 25, 26, 27, 28]. Ikeda and Miyake [28] have argued the physical properties of CeNiSn by the Fermi liquid theory of heavy fermions on the basis of the periodic Anderson model with a condition for the band insulator. The wave number k dependence of the hybridization matrix element was taken into account. In the case of the crystal electric field (CEF) ground state of $|J = 5/2, J_z = \mp 3/2\rangle$, which is expected in a trigonal symmetry, the hybridization matrix element vanishes along the a axis. As a result, the gap does not open in the a direction in the k space and a finite DOS intrinsically remains at a bottom of the gap.

Recently, Nakamoto *et al.* [29, 30, 31] succeeded in purification of single-crystalline samples of CeNiSn and experimentally shown that the electronic

properties are very sensitive to sample quality. In early works [5], electrical resistivity of CeNiSn rapidly increased below 6 K like a semiconductor with decreasing temperature. The increase in resistivity was believed to be the evidence of the gap formation. Therefore, CeNiSn was called a "Kondo insulator" or a "Kondo semiconductor". For purified samples, however, the semiconductor-like temperature variation changes to a metallic one, and the case is substantially different from other cubic compounds YbB_{12} and $Ce_3Bi_4Pt_3$ for which the increasing ratio of resistivity at low temperatures becomes larger by purification [32, 33]. The semiconductor-like conduction previously observed in CeNiSn is presumably due to carrier localization by impurities and/or imperfection. After purification, two impurity-peaks in specific heat vanished and T-independent value of C/T below 1 K decreased from 57 to 40 mJ/K^{2}mol. Ikeda and Miyake [28] showed theoretically that the shape of the gapped DOS around E_F is easily changed by impurity. In fact, the impurities might veil the intrinsic property in early samples. Thus, the sample quality is of essential importance for the study of this material.

A number of investigations have been performed on CeNiSn. However, the electronic ground state and the mechanism of the gap formation remains to be clarified. In this study, we measured specific heat and magnetocaloric effect from 0.1 to 25 K in magnetic field up to $\mu_0 H = 14$ T. Magnetic susceptibility measurement was performed from 2 to 600 K at 1 T. By using a high-quality single crystal, we observed a significant field effect in specific heat when magnetic field was applied parallel to the a axis, in contrast with nearly field-independent result for $H \parallel b$ and c. The results of specific heat and magnetic susceptibility were analyzed by a V-shaped gapped DOS model with residual DOS. From the obtained specific heat below 1 K, the electronic state at the bottom of the gap is discussed in terms of a new electronic state due to a many-body effect.

Chapter 2

Experimental

2.1 Sample preparation

Single crystals of CeNiSn used in this study were grown by a Czochralski technique using a radio-frequency furnace with a hot tungsten crucible in a purified Ar atmosphere. The crystals were purified by the technique of solid state electrotransport with current density of 600 A/cm^2 in a vacuum of 1×10^{-9} Torr for 16 days. The surface of the crystal was carefully polished because impurities on the surface results badly.

The impurity concentration of Ce_2O_3, $CeNi_2Sn_2$ and $Ce_2Ni_3Sn_2$ in the crystals has been confirmed less than 0.1 % by a metallographic examination and electron-probe microanalysis [29, 31]. Electrical resistivity ρ of the crystals shows metallic conduction for all axes at low temperatures. In comparison with unpurified sample, our sample exhibits the smallest ρ at 1.3 K along each a, b and c axis, indicating high quality.

2.2 Measurements

Molar specific heat C at a constant pressure was measured from 2 to 25 K in magnetic field up to 14 T using an adiabatic calorimeter with a mechanical heat switch, as shown in Fig. 2.1. The calorimeter was constructed in this study and was put into the variable temperature insert (VTI) of a cryostat with a 16 T

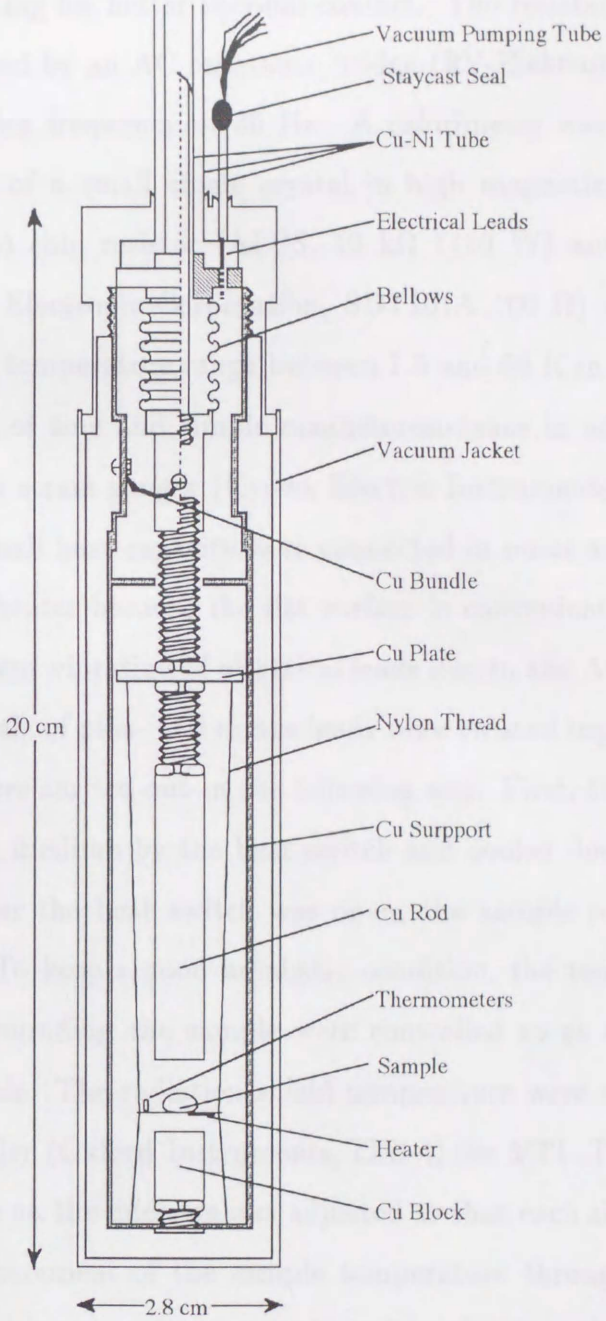

Figure 2.1: An adiabatic calorimeter designed for combination with a 16 T superconducting magnet.

superconducting solenoid (Oxford instruments). Thermometers and a heater were attached to a thin copper plate. The Cu plate is referred to as *addenda*. The sample ($1 \sim 2$ g) was placed on the *addenda* with grease (Apiezon Products

Limited, N grease) of 20 mg for better thermal contact. The resistance of the thermometer was measured by an AC resistance bridge (RV-Elektroniikka Oy, AVS-46) with an operating frequency of 30 Hz. A calorimeter was designed to measure specific heat of a small single crystal in high magnetic field. A Ruthenium-Oxide (RuO_2) chip resistor (ALPS, 10 kΩ 1/10 W) and a small platinum resistor (Tama Electronic Corporation, SDT101A 100 Ω) were used as a thermometer for the temperature range between 1.5 and 60 K in magnetic field up to 14 T because of tiny and simple magnetoresistance in addition to small heat capacity. Two strain gauges (Kyowa Electric Instruments, KFG-2-350-C1-23 350 Ω) with small heat capacity were connected in series and affixed to the Cu *addenda* as a heater because the flat surface is convenient for good thermal contact. To prevent vibration of electrical leads due to the AC current in the magnetic field, a pair of plus- and minus-leads were twisted together.

The measurements were carried out in the following way. First, the sample was connected to cooling medium by the heat switch and cooled down to the lowest temperature. After the heat switch was open, the sample remains in an adiabatic condition. To keep a good adiabatic condition, the temperature of a radiation shield surrounding the sample were controlled so as to be the same as that of the sample. The radiation shield temperature were controlled by a temperature controller (Oxford Instruments, ITC-4) for VTI. The power for heating up the sample on the *addenda* was adjusted so that each single heat pulse gives about 3 % increment of the sample temperature throughout the measurement. The total heat capacity was evaluated by dividing the applied heat by temperature difference between before and after heating. To obtain the exact heat capacity of samples, the heat capacity of the *addenda*, which was independently measured, was subtracted from the total heat capacity.

The measurements in the temperature range between 0.1 and 2 K were performed with an adiabatic calorimeter mounted under the mixing chamber of a

^{3}He-^{4}He dilution refrigerator. The *addenda* was connected to the mixing chamber through a superconducting heat switch. The superconducting heat switch was made of 6N lead foils with the dimensions of 140 × 2 × 0.1 mm. Two RuO_2 chips (ALPS, 1 kΩ 1/10 W) and one RuO_2 chip (ALPS, 4.7 kΩ 1/10 W) were included in the *addenda*. One RuO_2 chip of 1 kΩ was used as the heater and the rest chips of 1 kΩ and 4.7 kΩ as the thermometers. The external magnetic field up to 5 T was applied by a superconducting magnet. The magnet was made of Nb-Ti wire and covered with an iron jacket in order to reduce the magnetic field around the Pb heat switch. In the magnetic field, temperature was calculated with correction for the magnetoresistance of RuO_2 chip, which was also independently measured.

The magnetocaloric effect was measured by using the same equipment for the specific heat measurement.

The temperature variation of the sample in an adiabatic condition was measured with sweeping magnetic field at a constant rate of 0.14 T/min for the temperature range above 1 K.

A commercial SQUID magnetometer (Quantum Design Co., MPMS) was used to measure the magnetic susceptibility M/H along the a, b and c axes from 2 to 600 K at 1 T. The magnitude of applied field was evaluated from the magnetization of palladium which was independently calibrated in the same field.

Chapter 3

Results

3.1 Specific heat

3.1.1 Above 2 K

Figure 3.1 shows a ratio of specific heat to temperature C/T in selected magnetic fields of 0, 10 and 14 T along the a, b and c axes. No peak in C/T due to impurities is observed in this sample. Impurity peaks have always been

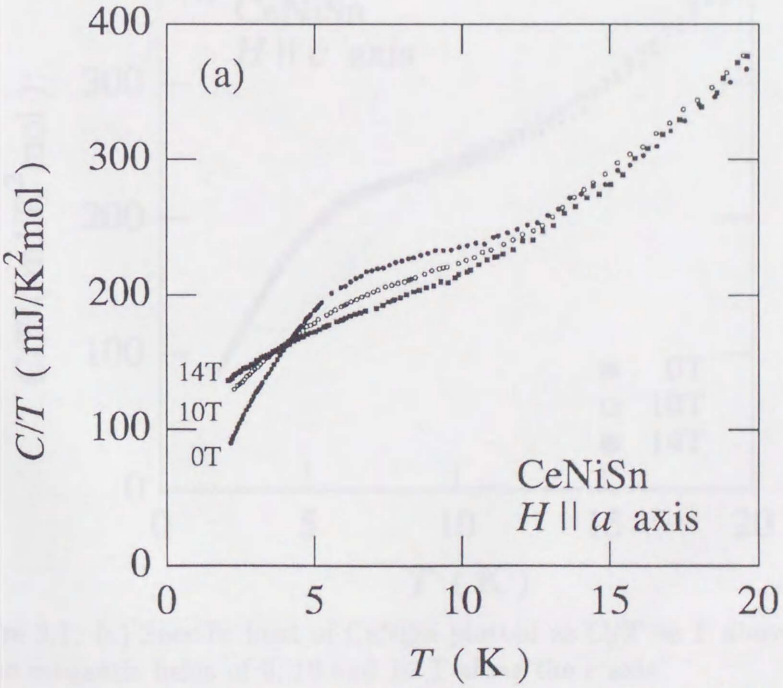

Figure 3.1: (a) Specific heat of CeNiSn plotted as C/T vs T above 2 K in the magnetic fields of 0, 10 and 14 T along the a axis.

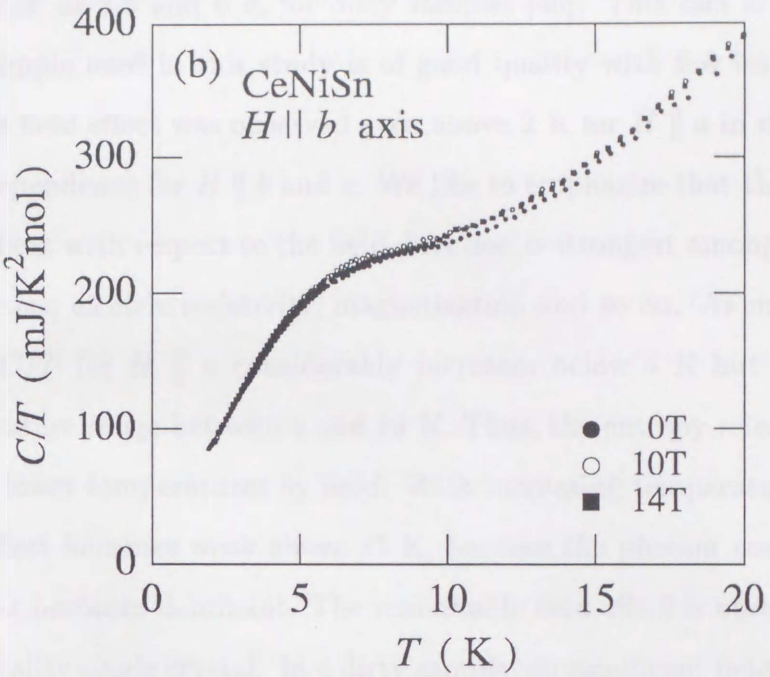

Figure 3.1: (b) Specific heat of CeNiSn plotted as C/T vs T above 2 K in the magnetic fields of 0, 10 and 14 T along the b axis.

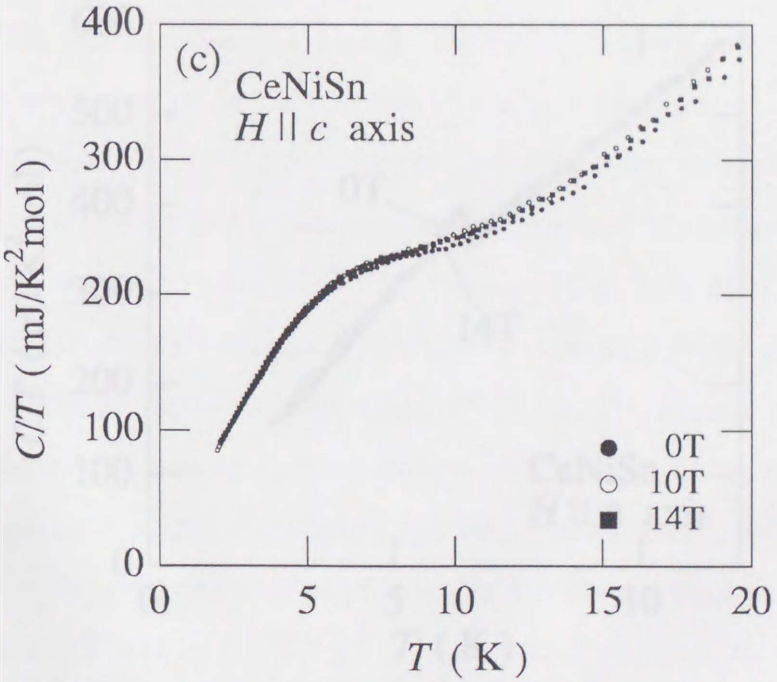

Figure 3.1: (c) Specific heat of CeNiSn plotted as C/T vs T above 2 K in the magnetic fields of 0, 10 and 14 T along the c axis.

found in C/T at 2.5 and 6 K for dirty samples [30]. This fact is an evidence that the sample used in this study is of good quality with few impurities. An appreciable field effect was observed even above 2 K for $H \parallel a$ in contrast with less field dependence for $H \parallel b$ and c. We like to emphasize that the anisotropy of specific heat with respect to the field direction is strongest among other physical properties; electric resistivity, magnetization and so on. As magnetic field increases, C/T for $H \parallel a$ considerably increases below 4 K but decreases in the temperature range between 4 and 14 K. Thus, the entropy release is caused to shift to lower temperatures by field. With increasing temperature, however, the field effect becomes weak above 15 K, because the phonon contribution to specific heat becomes dominant. The remarkable field effect is observed only in the high-quality single crystal. In a dirty sample, no significant field dependence was observed even for $H \parallel a$ as shown in Fig. 3.2. A peak is found in zero field at

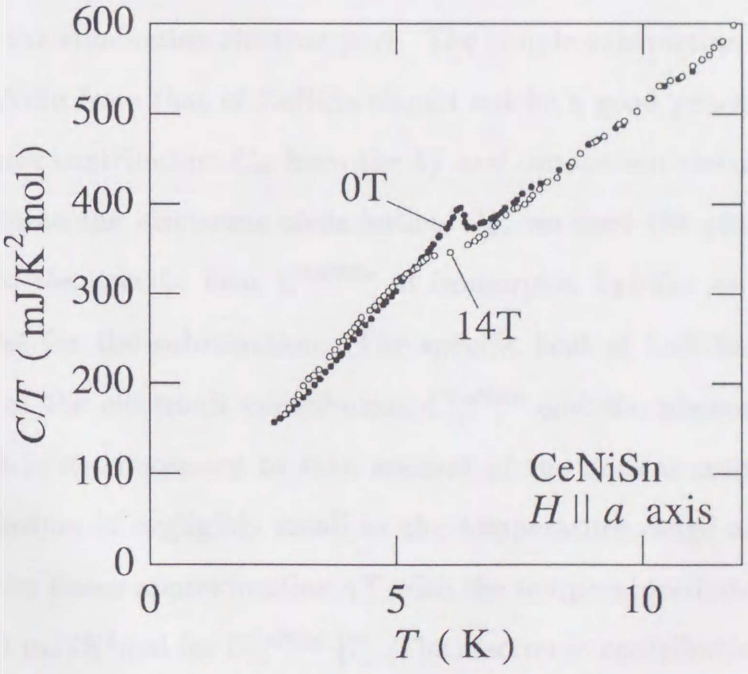

Figure 3.2: Temperature dependence of C/T for a dirty sample at 0 and 14 T along the a axis. Less field effect is observed in contrast to the result for the pure sample.

6 K and attributed to the magnetic ordering in the impurity phase of Ce_2O_3. In the field of 14 T, the peak is no longer observed because the magnetic ordering is suppressed by field.

In many studies of Ce-based compounds, the magnetic contribution C_m of $4f$ electrons to specific heat was used to discuss the electronic properties. To calculate C_m, one subtracts the specific heat of the isomorphic non magnetic compound without $4f$ electron from that of the Ce-based compound, for example, C of LaB_6 from C of CeB_6 [34]. In this calculation, not only the phonon part of C but also conduction-electron part of C is subtracted. This procedure is valid in the following two cases. (i) $4f$ electrons are strongly localized in the compound. (ii) C/T of the compound is quite large in comparison with that of a normal metal. In case of CeNiSn, since the Kondo temperature T_K is 51 K [7] and $C/T = \sim 40$ mJ/K^{2}mol at 0.1 K, the $4f$ electrons hybridize well with the conduction electrons in the temperature range below 25 K and it is difficult to neglect the conduction-electron part. The simple subtraction of the specific heat of LaNiSn from that of CeNiSn should not be a good procedure to obtain the electronic contribution C_{el} from the $4f$ and conduction electrons.

To evaluate the electronic contribution C_{el}, we used the phonon contribution C_{ph} to the specific heat C^{LaNiSn} of isomorphic LaNiSn as a background specific heat for the substraction. The specific heat of LaNiSn was assumed to consist of the electronic contribution C_{el}^{LaNiSn} and the phonon contribution C_{ph}^{LaNiSn}. It is not necessary to take account of the nuclear contribution since the contribution is negligibly small in the temperature range above 2 K. We employed the linear approximation γT with the temperature-independent value of $\gamma = 11.4$ mJ/K^{2}mol for C_{el}^{LaNiSn} [7]. The electronic contribution C_{el}^{CeNiSn} was evaluated by subtracting the phonon contribution as C_{ph}^{LaNiSn} $(= C^{\mathrm{LaNiSn}} - \gamma T)$ from the measured specific heat for CeNiSn. For the results in the finite magnetic field, we evaluated C_{el}^{CeNiSn} in the same way using the zero-field data of

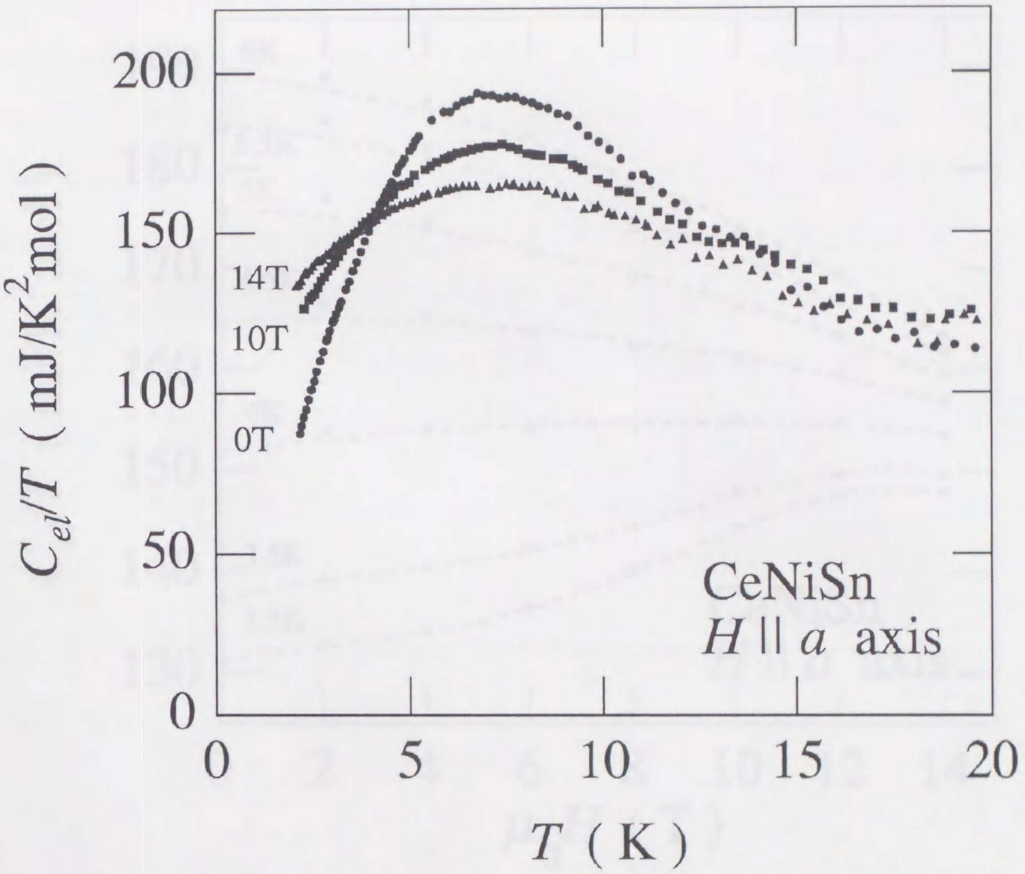

Figure 3.3: The ratio of electronic specific heat to temperature C_{el}/T of CeNiSn above 2 K in various magnetic fields parallel to the a axis.

LaNiSn, neglecting the field effect on C^{LaNiSn}.

In Fig. 3.3, C_{el}/T of CeNiSn is plotted as a function of temperature for selected fields $\mu_0 H = 0$, 10 and 14 T along the a axis. The increase in C_{el}/T from 20 to 7 K is caused by the enhancement of the DOS due to the growth of the Kondo resonance peak at E_{F} and then shows a maximum at 7 K. After marking the maximum, C_{el}/T rapidly decreases, indicating that the DOS reduces substantially within a narrow energy region around E_{F}. In order to show the effect of magnetic field more clearly, we plotted again the same data as a function of the field at several temperatures in Fig. 3.4. At 6 K, the value of C_{el}/T decreases

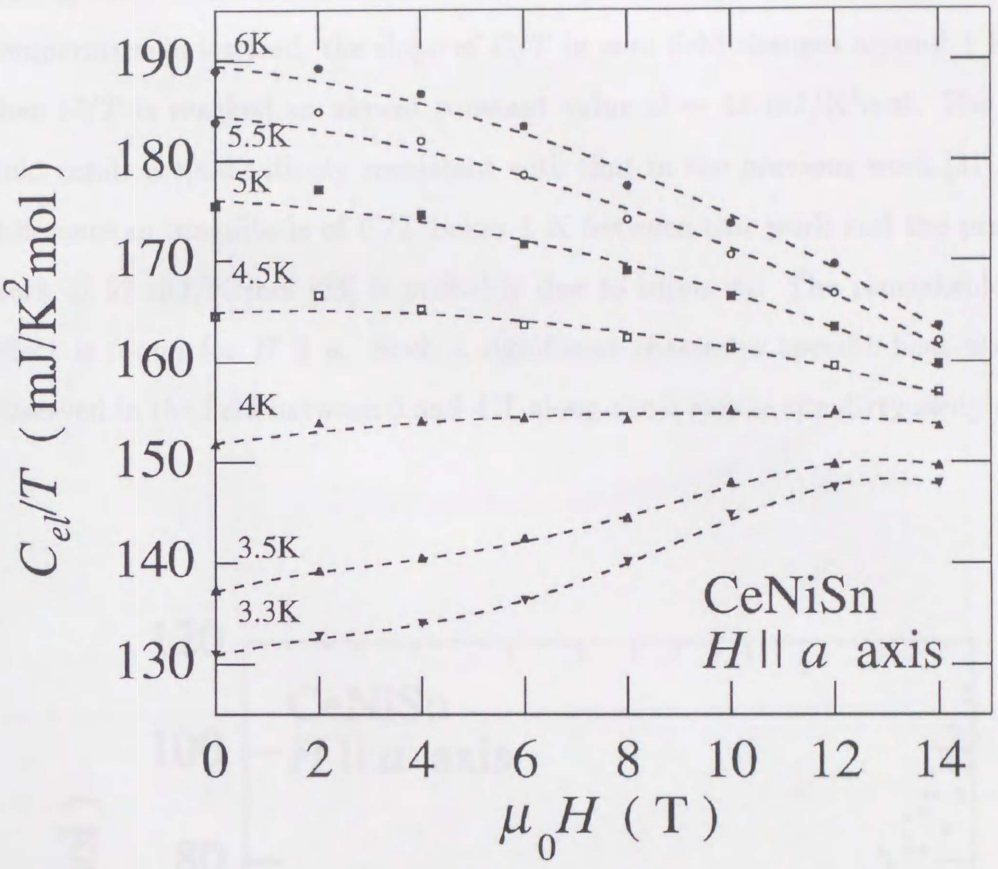

Figure 3.4: Field variation of C_{el}/T at several temperatures above 2 K. The dashed curves are guides for the eye.

with increasing field. As temperature is lowered, the field dependence of C_{el}/T is gradually weakened and the sign of the slope changes around 4 K. Finally, at 3.3 K, the C_{el}/T is an increasing function of H. Between 6 and 10 T, the slope of the C_{el}/T becomes steep below 4 K. This behavior is less obvious above 4 K. Around the corresponding field of around 10 T, metamagnetic behavior is reported in the study of the magnetization [18] and the elastic modulus [19]. The value of C_{el}/T below 3.5 K tends to level off at the highest field.

3.1.2 Below 2 K

The specific heat obtained below 2 K is plotted against T in Fig. 3.5. As temperature is lowered, the slope of C/T in zero field changes around 1 K and then C/T is reached an almost constant value of $\sim$ 42 mJ/K^{2}mol. The zero-field result is qualitatively consistent with that in the previous work [31]. The difference in magnitude of C/T below 1 K between this work and the previous work of 57 mJ/K^{2}mol [23] is probably due to impurity. The remarkable field effect is found for $H \parallel a$. Such a significant change in specific heat was not observed in the field between 0 and 4 T along the a axis in the dirty sample [23].

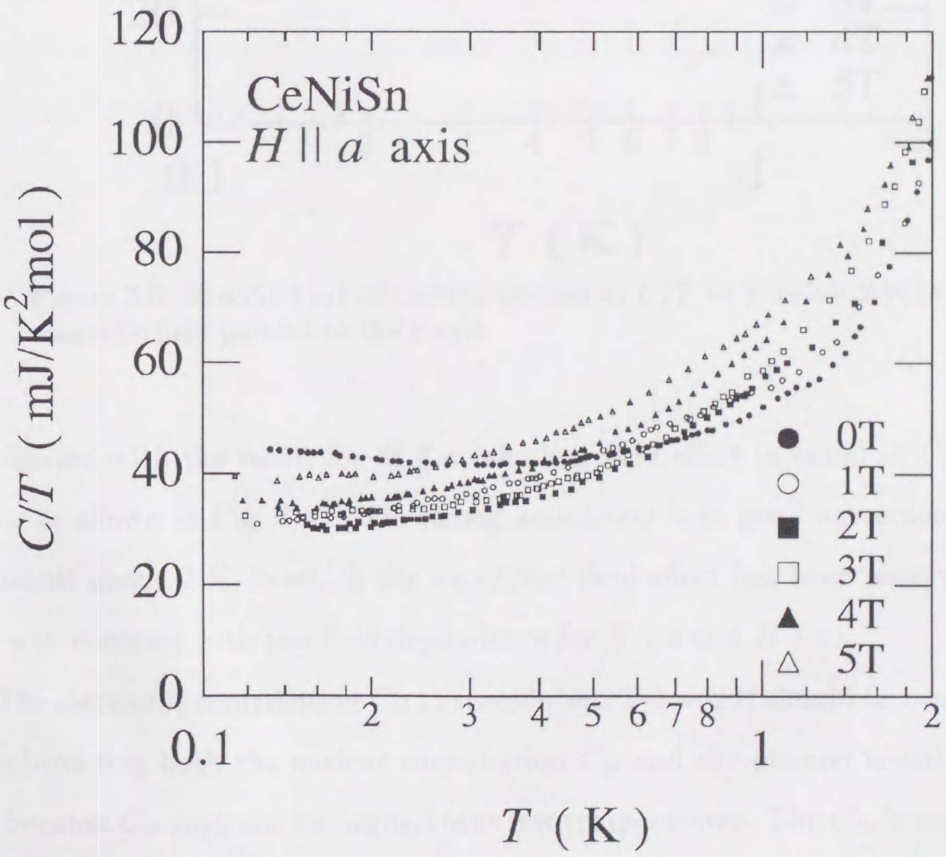

Figure 3.5: Specific heat divided by temperature C/T for CeNiSn below 2 K in magnetic field up to 5 T along the a axis.

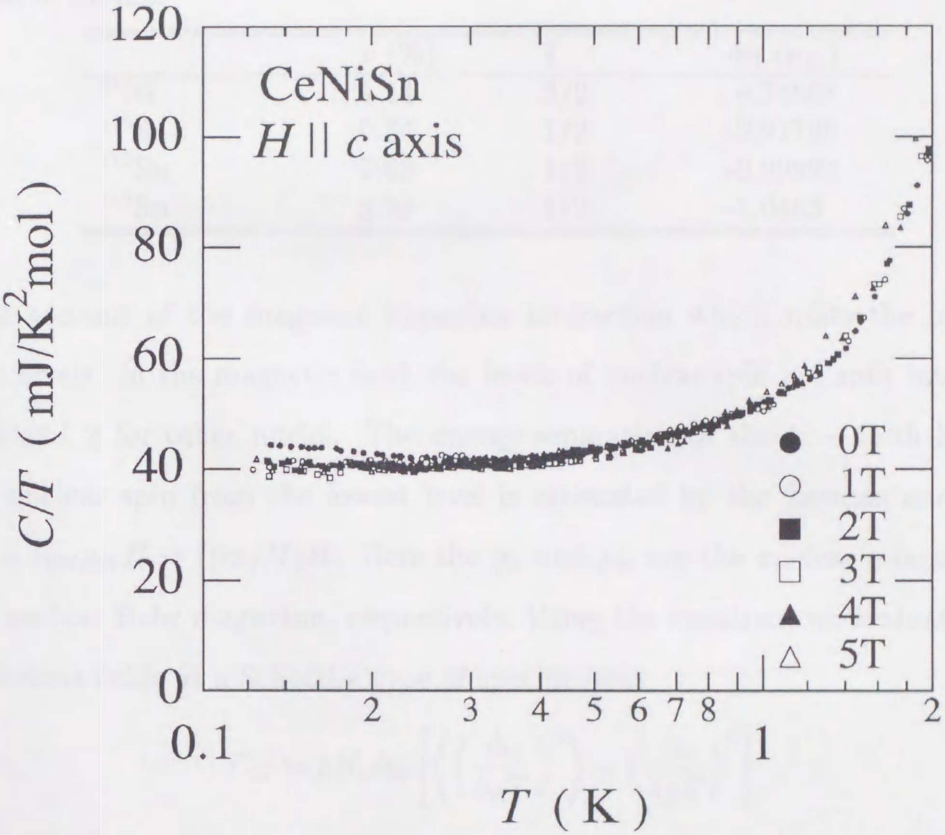

Figure 3.6: Specific heat of CeNiSn plotted as C/T vs T below 2 K in magnetic field parallel to the c axis.

In contrast with the result for $H \parallel a$, no clear field effect is found in C/T for $H \parallel c$ as shown in Fig. 3.6. This strong anisotropy is in good agreement with the result above 2 K, in which the significant field effect has been observed for $H \parallel a$ in contrast with less field dependence for $H \parallel b$ and $H \parallel c$.

The electronic contribution C_{el} to specific heat below 2 K should be evaluated by subtracting both the nuclear contribution C_N and the phonon contribution C_{ph} because C_N may not be negligible at low temperatures. The C_N is expected from the nuclear spin of ^{61}Ni, ^{115}Sn, ^{117}Sn and ^{119}Sn. Table 3.1 shows the natural abundance p, the nuclear spin I and the nuclear magnetic moment m_{I}

of these isotopes. Since no quadrupole moment exists in these nuclei, we only

Table 3.1: The isotopic abundance, nuclear spin and nuclear magnetic moment of the nuclei in CeNiSn

	p (%)	I	m_{I} (μ_N)
^{61}Ni	1.14	3/2	-0.74868
^{115}Sn	0.34	1/2	-0.91790
^{117}Sn	7.68	1/2	-0.99993
^{119}Sn	8.59	1/2	-1.0463

took account of the magnetic hyperfine interaction which splits the nuclear-spin levels. In the magnetic field, the levels of nuclear spin are split into 4 for ^{61}Ni and 2 for other nuclei. The energy separation of the $(i-1)$-th level of the nuclear spin from the lowest level is estimated by the Zeeman energy as $\Delta_i = ig_N\mu_N H = i(m_I/I)H$. Here the g_{N} and μ_{N} are the nuclear g-factor and the nuclear Bohr magneton, respectively. Using the equation, we evaluated C_N in various fields as a Schottky type of specific heat:

$$C_N = pN_{\mathrm{A}}k_{\mathrm{B}}\left[\left\langle\left(\frac{\Delta_i}{k_{\mathrm{B}}T}\right)^2\right\rangle - \left\langle\frac{\Delta_i}{k_{\mathrm{B}}T}\right\rangle^2\right] \tag{3.1}$$

where the bracket denotes a mean quantity Q as

$$\langle Q\rangle = \sum_i \frac{Q\exp\left(\frac{\Delta_i}{k_{\mathrm{B}}T}\right)}{1+\sum_i \exp\left(\frac{\Delta_i}{k_{\mathrm{B}}T}\right)}. \tag{3.2}$$

The N_{A} and k_{B} are the Avogadro number and the Boltzmann constant, respectively. The amount of evaluated C_N is about 7 % of total specific heat at 0.15 K in a magnetic field of 5 T.

The phonon contribution was estimated as $C_{ph} = \beta T^3$, because the specific heat of LaNiSn is well reproduced by $\gamma T + \beta T^3$ at low temperatures. The amount of C_{ph} is less than 1 % of total specific heat at 1 K. The $\beta = 0.49$ mJ/K^{4}mol [7] was assumed to be field independent.

The evaluated value of C_{el}/T for $H \parallel a$ and c versus T is plotted in Fig. 3.7 and 3.8, respectively. In zero field, C_{el}/T exhibits a slight increase below 0.5 K

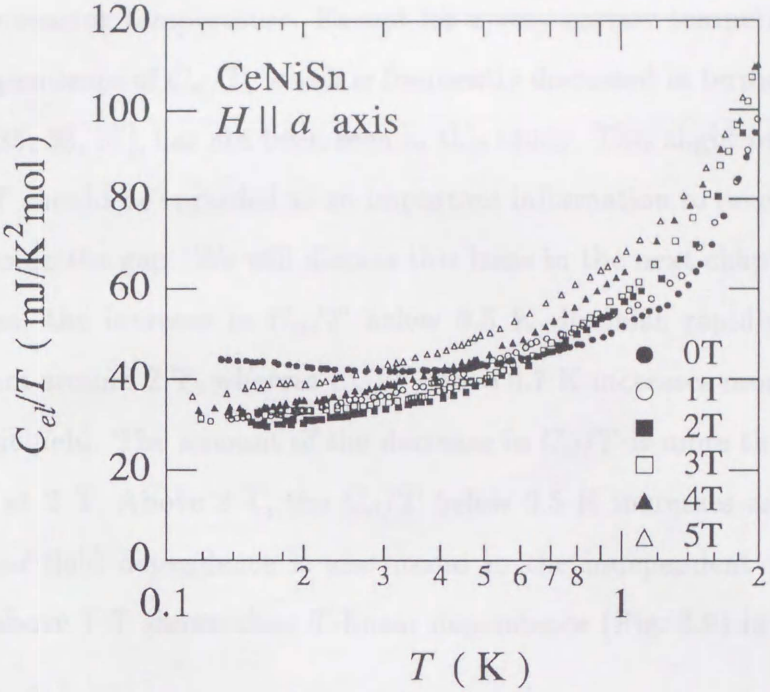

Figure 3.7: Temperature dependence of C_{el}/T of CeNiSn below 2 K for $H \parallel a$.

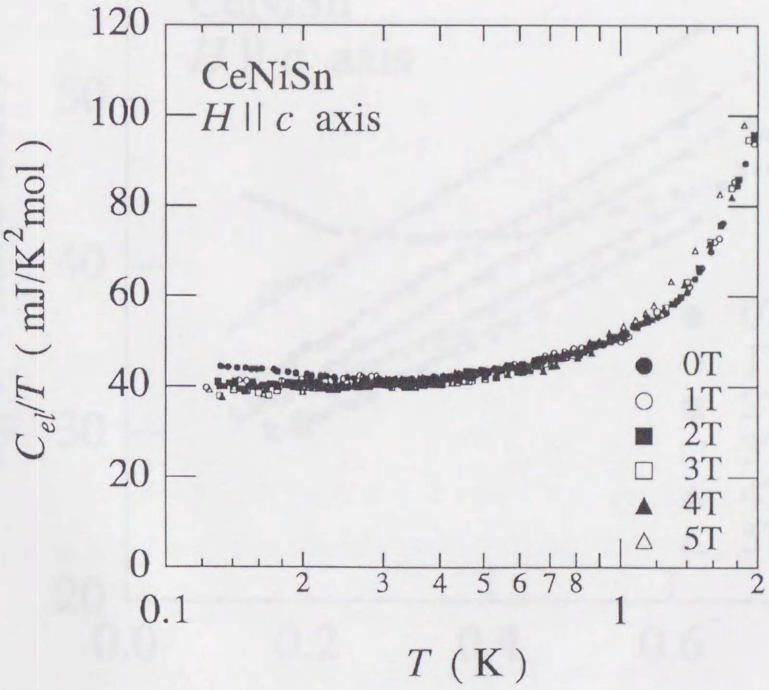

Figure 3.8: The C_{el}/T of CeNiSn plotted as a function of H in selected temperature below 2 K.

with decreasing temperature. Except for a very narrow temperature range, the $\ln T$-dependence of C_{el}/T, which is frequently discussed in terms of a non-Fermi liquid [35, 36, 37], has not been seen in this study. This slight but clear increase of C_{el}/T should be regarded as an important information to reveal the electronic state inside the gap. We will discuss this issue in the next chapter. As the field increases, the increase in C_{el}/T below 0.5 K diminish rapidly and attains a minimum around 2 T, whereas C_{el}/T above 0.7 K increases monotonically with magnetic field. The amount of the decrease in C_{el}/T is more than 30 % around 0.15 K at 2 T. Above 2 T, the C_{el}/T below 0.5 K increases as field increases. A similar field dependence is also found in the independent work [38]. The C_{el}/T above 1 T shows clear T-linear dependence (Fig. 3.9) in contrast to the

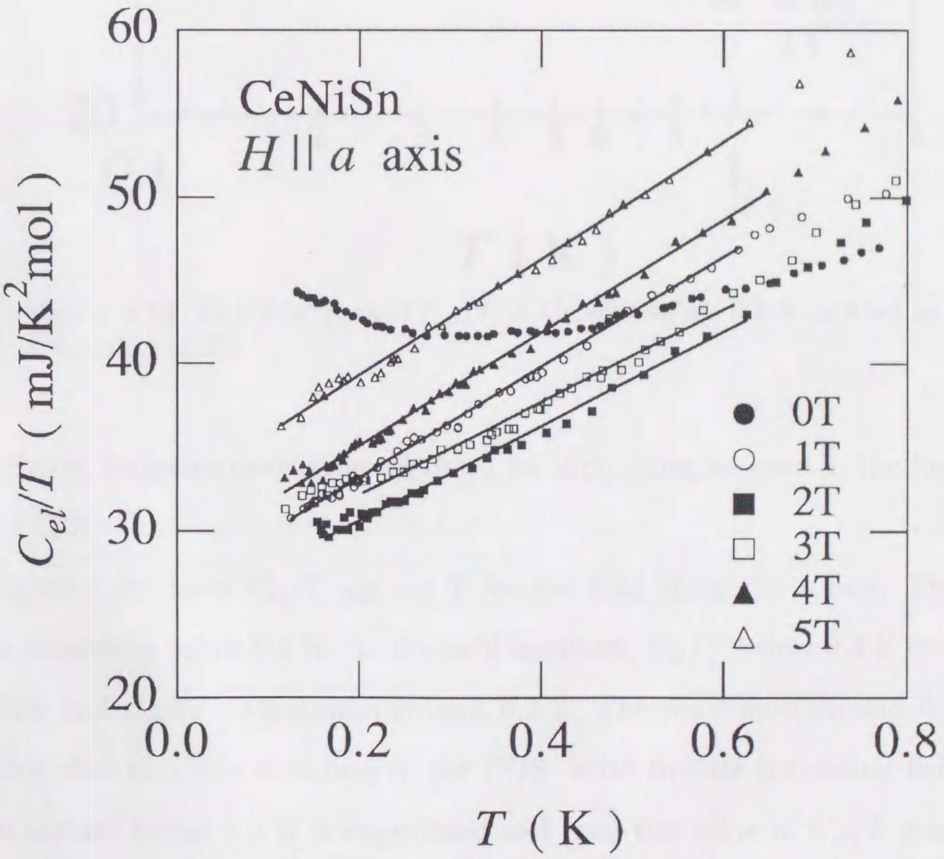

Figure 3.9: The C_{el}/T of CeNiSn for $H \parallel a$ below 2 K in linear T scale. The solid lines are guides for the eye.

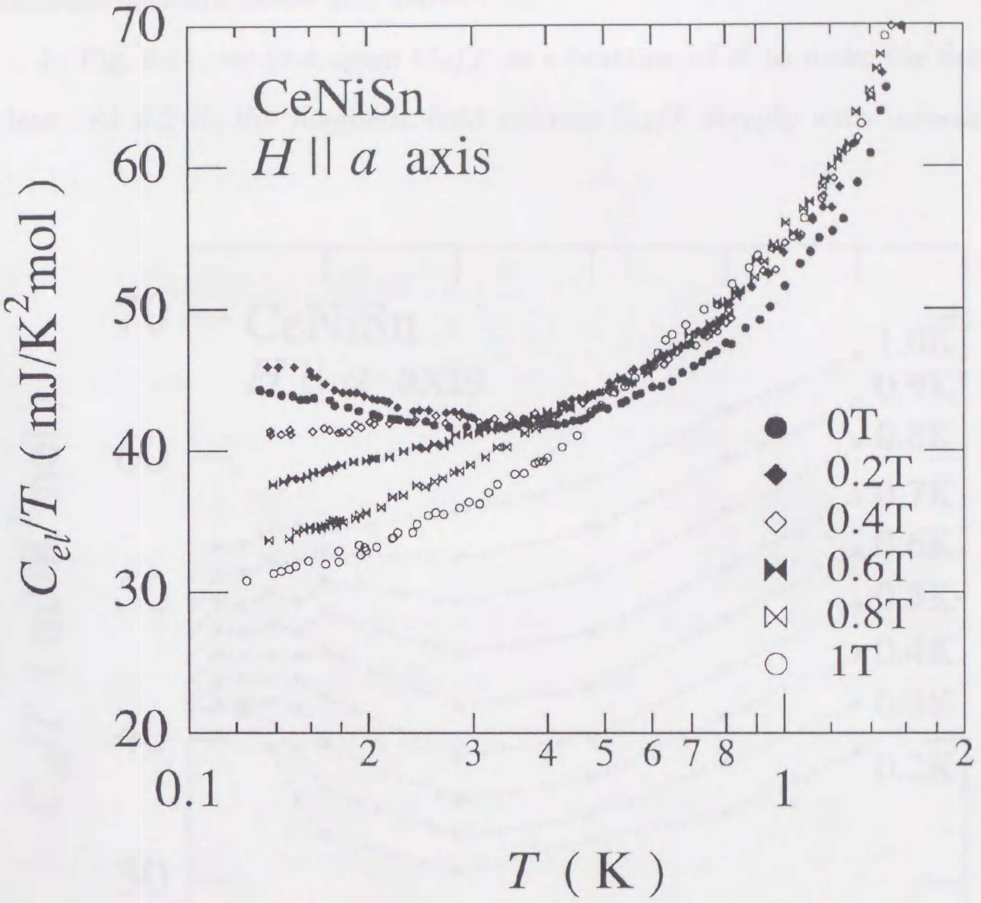

Figure 3.10: Low field part of C_{el}/T of CeNiSn below 0.8 K plotted as a function of T.

T-constant behavior previously reported for dirty samples even in the fields up to 5 T [23].

Figure 3.10 shows C_{el}/T against T for low field along the a axis. The field effect is obvious below 0.5 K. As the field increases, C_{el}/T below 0.3 K increases initially and shows a maximum around 0.2 T. The maximum around 0.2 T is possibly due to a fine structure of the DOS. With further increasing field, the slight upturn below 0.5 K is suppressed and then the value of C_{el}/T gradually decreases down to the value for 1 T. On the other hand, the C_{el}/T above 0.5 K is hardly affected by the field. The field effect is qualitatively different from that

for above 1 T. The difference suggests that the origin of the field dependence is different between below and above 1 T.

In Fig. 3.11, we plot again C_{el}/T as a function of H to make the field effect clear. At 0.2 K, the magnetic field reduces C_{el}/T steeply with increasing the

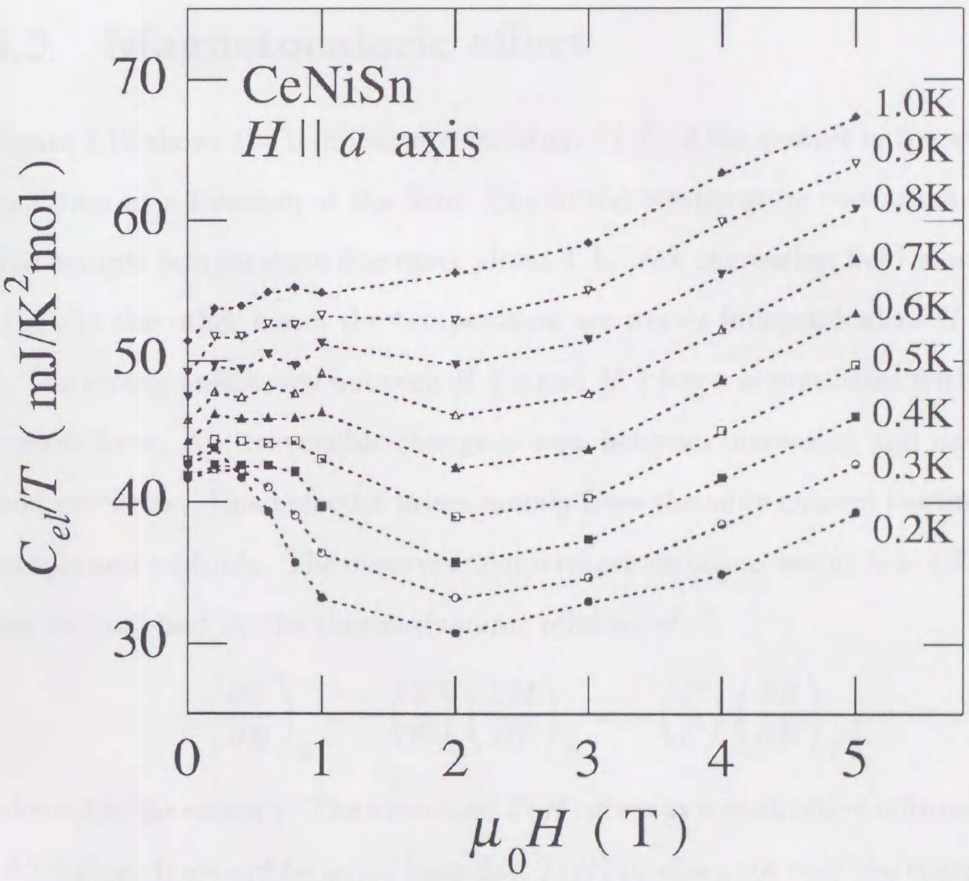

Figure 3.11: Magnetic field dependence of C_{el}/T of CeNiSn in selected temperature below 2 K. The dashed curves are guides for the eye.

field up to 1 T. Above 1 T, the variation of C_{el}/T becomes gradual with increasing field and then exhibits a minimum value around 2 T. Above 2 T, C_{el}/T increases monotonically. With elevating temperature, the field dependence becomes smooth. Especially, the low field structure is smeared out at 0.5 K. No decrease is observed in the filed dependence of C_{el}/T above 0.7 K. In the recent result of the longitudinal magnetoresistance along the a axis [39], a minimum

and a peak of Gaussian-type have been found below 0.3 K at 0.2 and 0.77 T, respectively. At 0.2 T where the magnetoresistance shows the minimum, C_{el}/T shows the maximum. Around 0.77 T, the decreasing rate in C_{el}/T becomes a maximum. The close correspondence between magnetoresistance and C_{el}/T in field may be attributed to a field induced change in the DOS.

3.2 Magnetocaloric effect

Figure 3.12 shows the temperature variation $T(H)$ of the sample in the adiabatic condition as a function of the field. The initial temperature was around 3.5 K. The sample temperature decreases about 1 K with increasing field along the a axis. On the other hand, the temperature are nearly independent of $H \parallel b$ and c. The strong anisotropy between $H \parallel a$ and $H \parallel b$ or c is consistent with that of specific heat. An irreversible change is seen between increasing and decreasing field processes. This behavior arises mainly from the eddy current heating of the sample and *addenda*. The observed temperature variation versus field $(\partial T/\partial H)_S$ can be analyzed by the thermodynamic relation of

$$\left(\frac{\partial T}{\partial H}\right)_S = -\left(\frac{T}{C}\right)\left(\frac{\partial M}{\partial T}\right)_H = -\left(\frac{T}{C}\right)\left(\frac{\partial S}{\partial H}\right)_T, \tag{3.3}$$

where S is the entropy. The measured $T(H)$ gives us a qualitative information on $(\partial S/\partial H)_T$. It should be noted here that $T(H)$ involves not only the contribution of the sample but also that of *addenda*. The contribution of *addenda* to $T(H)$ can be neglected because only a small variation of $T(H)$ was confirmed for the *addenda* by independent measurements. The decrease of the sample temperature from 3.5 K, that is $(\partial T/\partial H)_S < 0$, indicates that the entropy is enhanced by the field along the a axis. The enhancement of the entropy is consistent with the result of the specific heat measurement in magnetic field, which exhibits that the release of entropy shifts to lower temperature below 4 K in the presence of field.

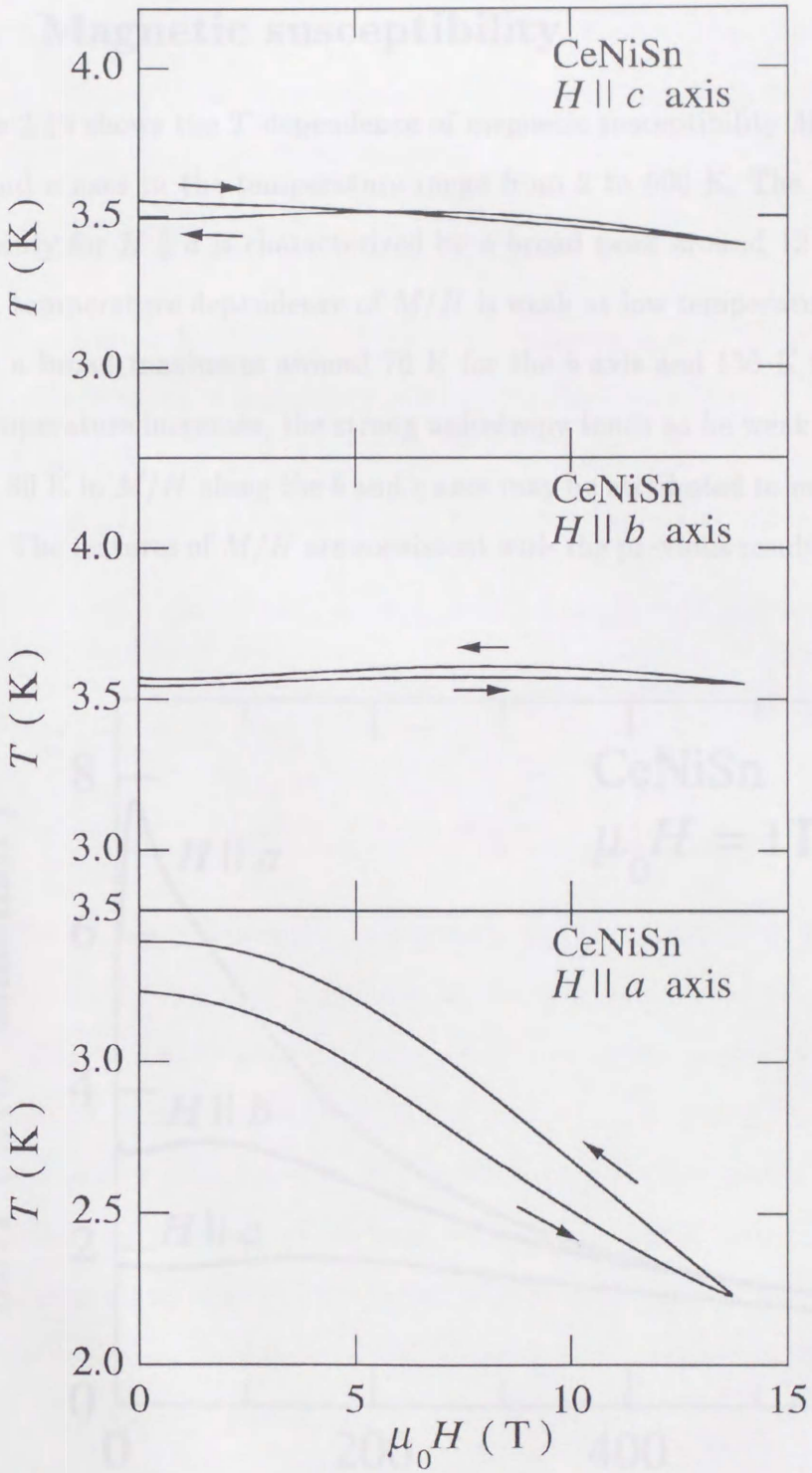

Figure 3.12: Temperature variation $T(H)$ of CeNiSn in adiabatic condition plotted against H.

3.3 Magnetic susceptibility

Figure 3.13 shows the T dependence of magnetic susceptibility M/H along the a, b and c axes in the temperature range from 2 to 600 K. The magnetic susceptibility for $H \parallel a$ is characterized by a broad peak around 12 K. For $H \parallel b$ and c, temperature dependence of M/H is weak at low temperatures and M/H shows a broad maximum around 70 K for the b axis and 150 K for the c axis. As temperature increases, the strong anisotropy tends to be weak. The upturns below 30 K in M/H along the b and c axes may be attributed to magnetic impurities. The features of M/H are consistent with the previous results below 300 K

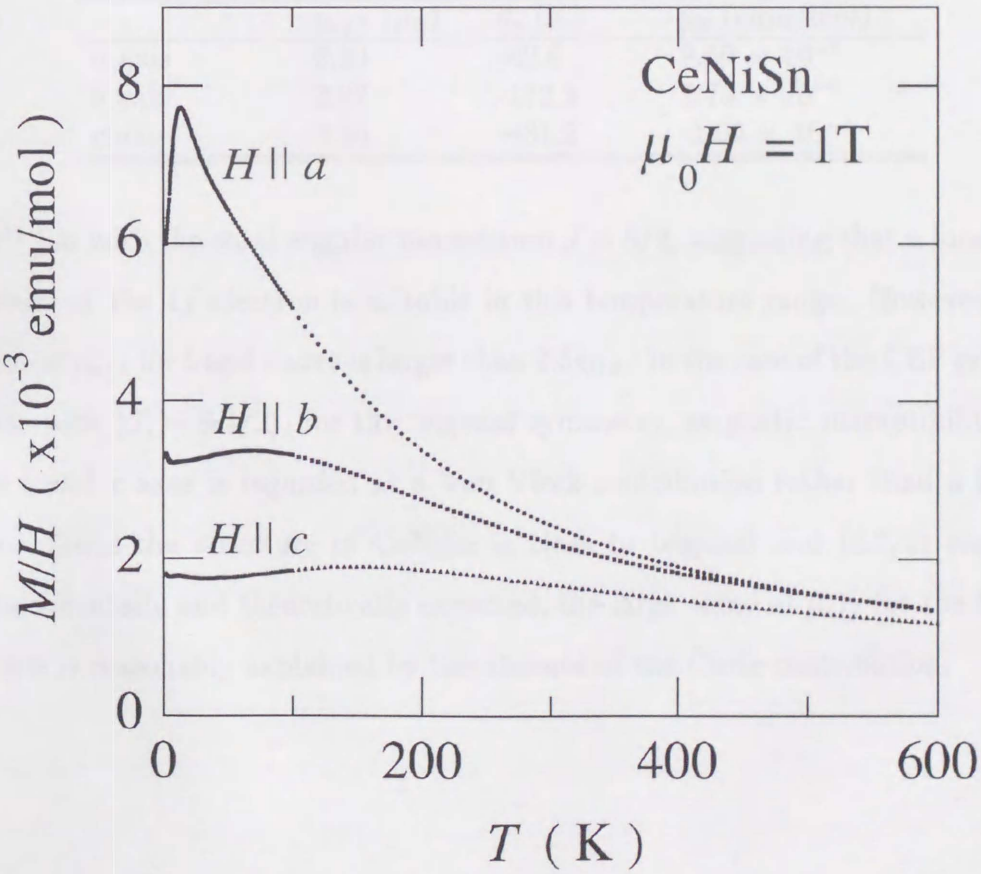

Figure 3.13: Temperature variation of magnetic susceptibility M/H of CeNiSn up to 600 K

[31]. Above 300 K, M/H can be described by a Curie-Weiss type temperature variation. Fitting of M/H is performed for temperature range between 340 and 560 K by using the Curie-Weiss formula,

$$\chi = \frac{C}{T - \theta_p} + \chi_0, \tag{3.4}$$

where C and θ_p are the Curie constant and the paramagnetic Curie temperature, respectively, and χ_0 is a temperature independent contribution. The effective moment μ_{eff}, θ_p and χ_0 obtained for $H \parallel a$, b and c are shown in Table 3.2. The value of $\mu_{eff} = 2.53\mu_B$ is close to the theoretical value $2.54\mu_B$ for the free

Table 3.2: List of the effective moment, the paramagnetic Curie temperature and T-independent contribution

	μ_{eff} (μ_B)	θ_p (K)	χ_0 (emu/mol)
a axis	2.53	-42.6	9.50×10^{-5}
b axis	2.87	-172.3	2.73×10^{-5}
c axis	3.34	-481.2	-1.05×10^{-4}

Ce^{3+} ion with the total angular momentum $J = 5/2$, suggesting that a localized picture of the $4f$ electron is suitable in this temperature range. However, the value of μ_{eff} for b and c axes is larger than $2.54\mu_B$. In the case of the CEF ground state with $|J_z = \pm 3/2\rangle$, for the trigonal symmetry, magnetic susceptibility for the b and c axes is regarded as a Van Vleck contribution rather than a Curie one. Since the structure of CeNiSn is close to trigonal and $|\pm 3/2\rangle$ state is experimentally and theoretically expected, the large value of μ_{eff} for the b and c axes is reasonably explained by the absence of the Curie contribution.

Chapter 4

Discussion

In this chapter, the obtained specific heat is analysed by using a modified DOS model with a V-shaped gap and a residual DOS. The effect of the magnetic field on the pseudo-gap is discussed by the Zeeman energy. We use this model to demonstrate the origin of the peak in the magnetic susceptibility at 12 K. The field dependence of specific heat below 1 K is describable if we assume that a new many-body state is formed at the bottom of the pseudo-gap.

4.1 Magnetic field effect on the pseudo-gap

In order to analyze the T and H dependence of C_{el}/T, we modify the previous DOS model proposed in the reference [6] and [7]. We add a residual DOS to the V-shaped gap as illustrated in Fig. 4.1(a). Temperature dependence of the DOS shape is neglected in the present model. Furthermore, we assume that the field dependence of C_{el} is caused only by the Zeeman interaction, $E_{\mathrm{Zeeman}} = \pm g_J |J_z| \mu_B H$, where g_J, J_z and μ_B are the Landé g-factor, the z component of total angular momentum and the Bohr magneton, respectively. In the magnetic field, the total DOS $N(E)$ splits into the partial DOS, $N^+(E)$ and $N^-(E)$ for the up- and down-spin bands. A schematic DOS profile in magnetic field is sketched in Fig. 4.1(b), where the dotted and the broken curves indicates the N^+ and N^-, respectively. As the field increases, the $N(E)$ drawn by the solid

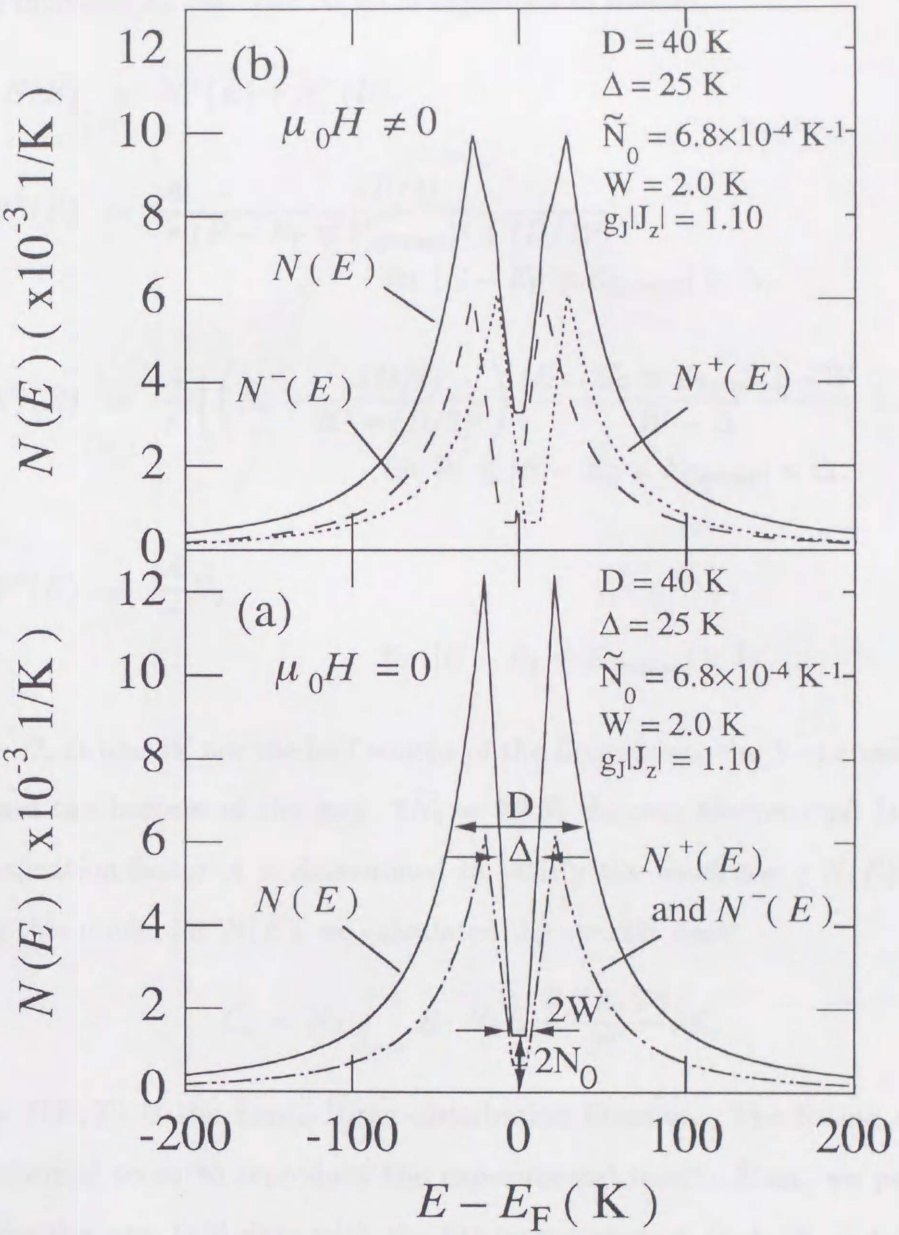

Figure 4.1: Schematic DOS profile with a pseudo-gap. The parameters D, Δ, W and $\tilde{N}_0$ are half-widths of the Lorentzian, the V-shaped gap and the bottom of the gap, and the magnitude of the residual DOS, respectively. The dotted curve is the DOS for up-spin and the broken curve is for down-spin, and the solid curve is the total DOS, $N(E)$. (a) In zero field, the DOS of the up- and down-spins, $N^+(E)$ and $N^-(E)$, overlap each other. (b) In magnetic field, the DOS of up- and down-spins shift upward and downward due to the Zeeman interaction, respectively, and the total DOS around E_F increases.

curve increases at $E_{\rm F}$. The $N(E)$ is expressed as follows,

$$N(E) = N^{+}(E) + N^{-}(E), \tag{4.1}$$

$$N^{\pm}(E) = \frac{A}{\pi}\frac{(D/2)}{(E - E_{\rm F} \mp E_{\rm Zeeman})^2 + (D/2)^2} \quad \text{for } |E - E_{\rm F} \mp E_{\rm Zeeman}| \geq \Delta, \tag{4.2}$$

$$N^{\pm}(E) = \frac{A}{\pi}\left\{\left(N_0 - \frac{(D/2)}{\Delta^2 + (D/2)^2}\right)\frac{|E - E_{\rm F} \mp E_{\rm Zeeman}| - W}{W - \Delta} + N_0\right\} \quad \text{for } W \leq |E - E_{\rm F} \mp E_{\rm Zeeman}| < \Delta, \tag{4.3}$$

$$N^{\pm}(E) = \frac{A}{\pi}N_0 \quad \text{for } |E - E_{\rm F} \mp E_{\rm Zeeman}| < W, \tag{4.4}$$

where D, Δ and W are the half widths of the Lorentzian, the V-shaped pseudo-gap and the bottom of the gap. $2\widetilde{N_0} = 2\frac{A}{\pi}N_0$ denotes the residual DOS. The normalization factor A is determined to satisfy the condition $\int N(E)dE = 1$. Using this model for $N(E)$, we calculated the specific heat

$$C_{el} = N_A \int_{-\infty}^{\infty} E \cdot N(E)\frac{\partial f(E,T)}{\partial T}dE, \tag{4.5}$$

where $f(E,T)$ is the Fermi-Dirac distribution function. The fitting of C_{el}/T is performed so as to reproduce the experimental result. First, we performed a fit for the zero field data with the fitting parameters D, Δ, W and N_0. The best fit is obtained with the parameter D = 40 K, Δ = 25 K, W = 2.0 K, $\widetilde{N_0} = \frac{A}{\pi}N_0 = 6.8 \times 10^{-4}$ K^{-1}. The fitted curve reproduces the experimental C_{el}/T very well as shown in Fig. 4.2. It should be noted that the same values of D, Δ, W and N_0 for zero field are also well reproduce C_{el}/T even in the magnetic field up to 14 T with the parameter $g_J|J_z| = 1.10$. The good fit obtained with a single set of parameters for various magnetic fields reveals that the Kondo-resonance peak in the DOS as well as the V-shaped pseudo-gap for both

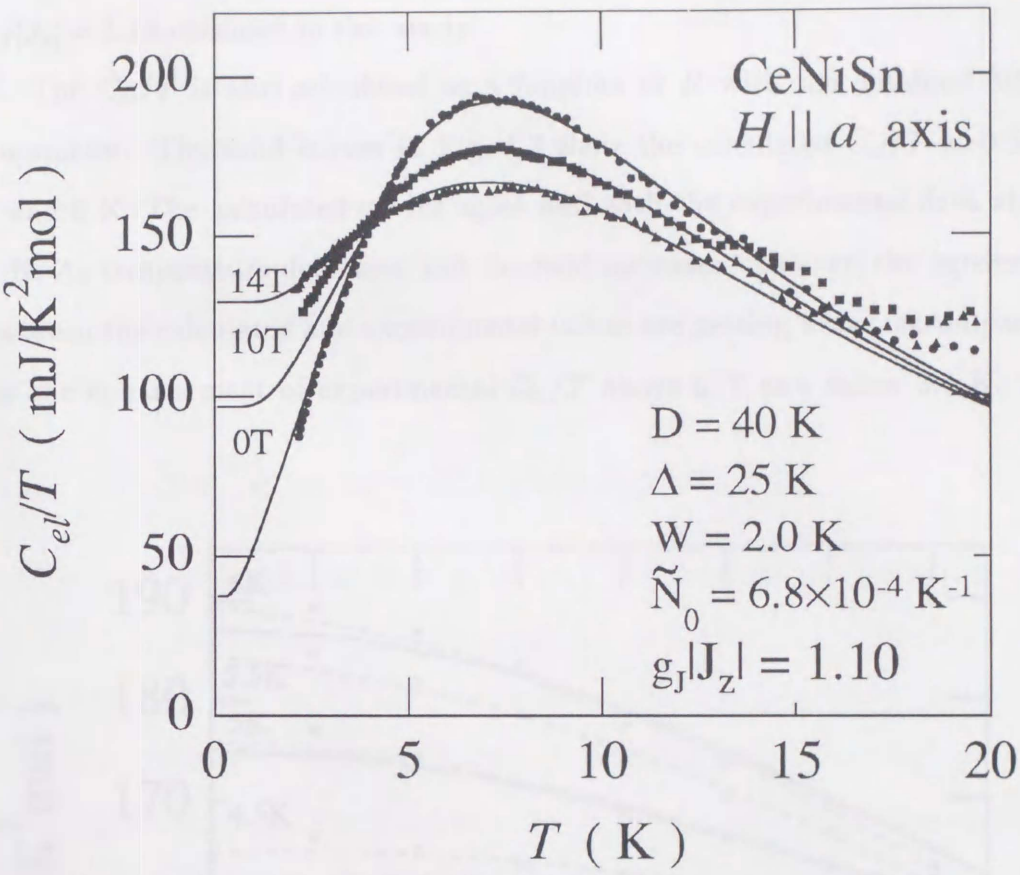

Figure 4.2: Fitting by the DOS model. The solid curves show the calculated C_{el}/T for 0, 10 and 14 T by using the DOS illustrated in Fig. 4.1.

up- and down-spin is hardly affected by the field at least up to 14 T although effect of magnetic field on the pseudo-gap has been unclear until this study. In other words, a rigid band picture is valid for the temperature range above 2 K in the field up to 14 T. This conclusion is understood from the viewpoint of energy-scale comparison between the Kondo and Zeeman interaction as $T_{\rm K}$ = 51 K $> E_{\rm Zeeman}/k_{\rm B} \simeq 10$ K at 14 T.

Ikeda and Miyake [28] argued that the CEF state of $|J = 5/2, J_z = \pm 3/2\rangle$ is the basis of the ground state of CeNiSn. The ultrasonic measurement for the isostructural CePtSn [40] suggests that the $|5/2, \pm 3/2\rangle$ term is dominant for the obtained ground state. For the CEF state of $|5/2, \pm 3/2\rangle$, the value of

$g_J|J_z|$ is expected to be 1.29. This value is in reasonable agreement with the $g_J|J_z| = 1.10$ obtained in this study.

The C_{el}/T is also calculated as a function of H with the obtained fitting parameter. The solid curves in Fig. 4.3 show the calculated C_{el}/T at 3.5, 4, 5 and 6 K. The calculated curves agree well with the experimental data above 4 K. As temperature decreases and the field increases, however, the agreement between the calculated and experimental values are getting worse, accompanied by the enhancement of experimental C_{el}/T above 6 T and below 3.5 K. The

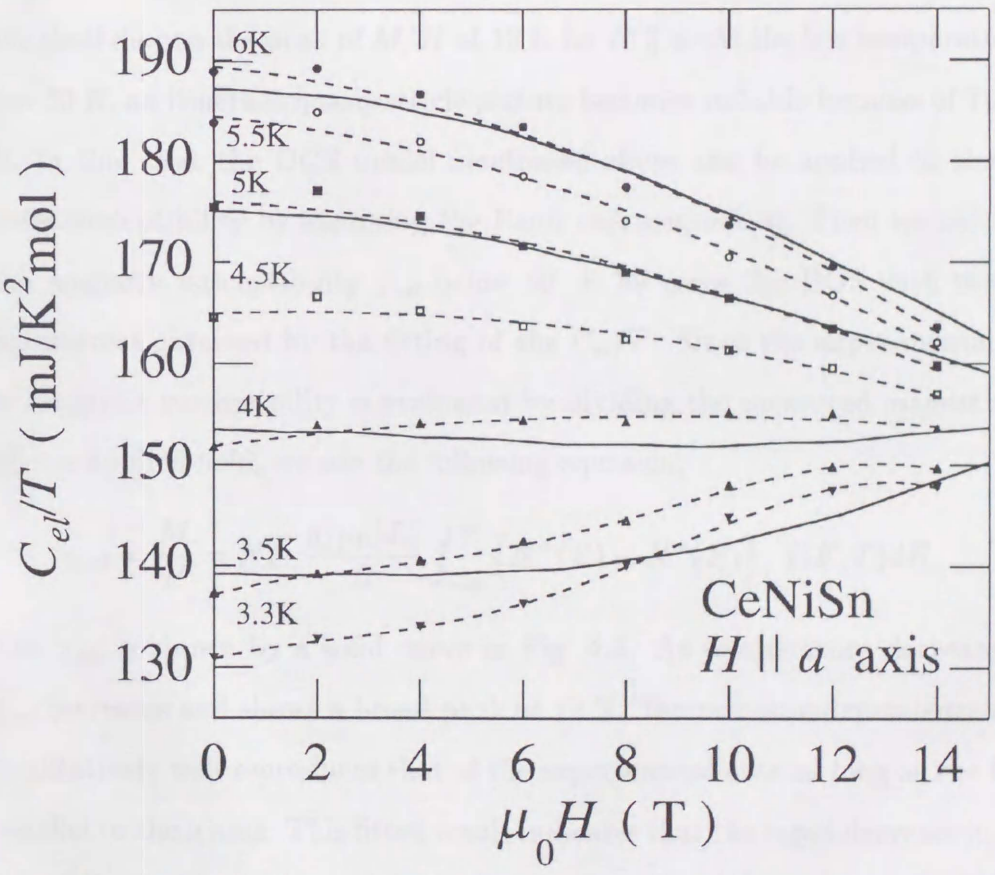

Figure 4.3: Fitting of C_{el}/T as a function of H. The solid curves are calculated H dependence of C_{el}/T for CeNiSn at temperatures of 3.5, 4, 5 and 6 K using the parameters shown in Fig. 4.2. The dashed curves are guides for the eye.

discrepancy probably arises from the simple and rigid structure of the DOS model, which suggests that a fine structure exists inside the pseudo-gap and/or that the pseudo-gap is dynamically changed at the higher fields. Recently, Saso [41, 42] theoretically discussed temperature and field dependence of the pseudo-gap of CeNiSn. In the theory, the rigid gap picture is valid at low field. With further increasing field, however, the gap collapses dynamically after the bottom edge ($E = \pm W$) crosses $E_{\rm F}$. The disagreement at high field may correspond to his story.

4.2 Peak in magnetic susceptibility

We shall discuss the peak of M/H at 12 K for $H \parallel a$. At the low temperature below 50 K, an itinerant quasiparticle picture becomes suitable because of $T_{\rm K} = 51$ K. In this case, the DOS model mentioned above can be applied to the magnetic susceptibility by assuming the Pauli paramagnetism. Then we calculated the magnetic susceptibility χ_{cal} below 50 K by using the DOS with the same parameters obtained by the fitting of the C_{el}/T. Since the experimental value of magnetic susceptibility is evaluated by dividing the measured magnetization by the applied field, we use the following equation,

$$\chi_{cal} = \frac{M}{H} = N_{\rm A} \cdot \frac{g_J \mu_{\rm B} |J_z|}{H} \int_{-\infty}^{\infty} \left\{ N^-(E) - N^+(E) \right\} \cdot f(E,T) dE. \qquad (4.6)$$

The χ_{cal} is shown by a solid curve in Fig. 4.4. As temperature decreases, the χ_{cal} increases and shows a broad peak at 12 K. Temperature dependence of χ_{cal} qualitatively well reproduces that of the experimental data as long as the field is parallel to the a axis. This fitted result indicates that the rapid decrease in M/H below 12 K is not due to the development of an antiferromagnetic correlation but rather due to the decrease of the DOS *i.e.* the development of the pseudo-gap. The difference in the absolute value between χ_{cal} and the experimental data is responsible for almost T-independent contribution such as the Van Vleck

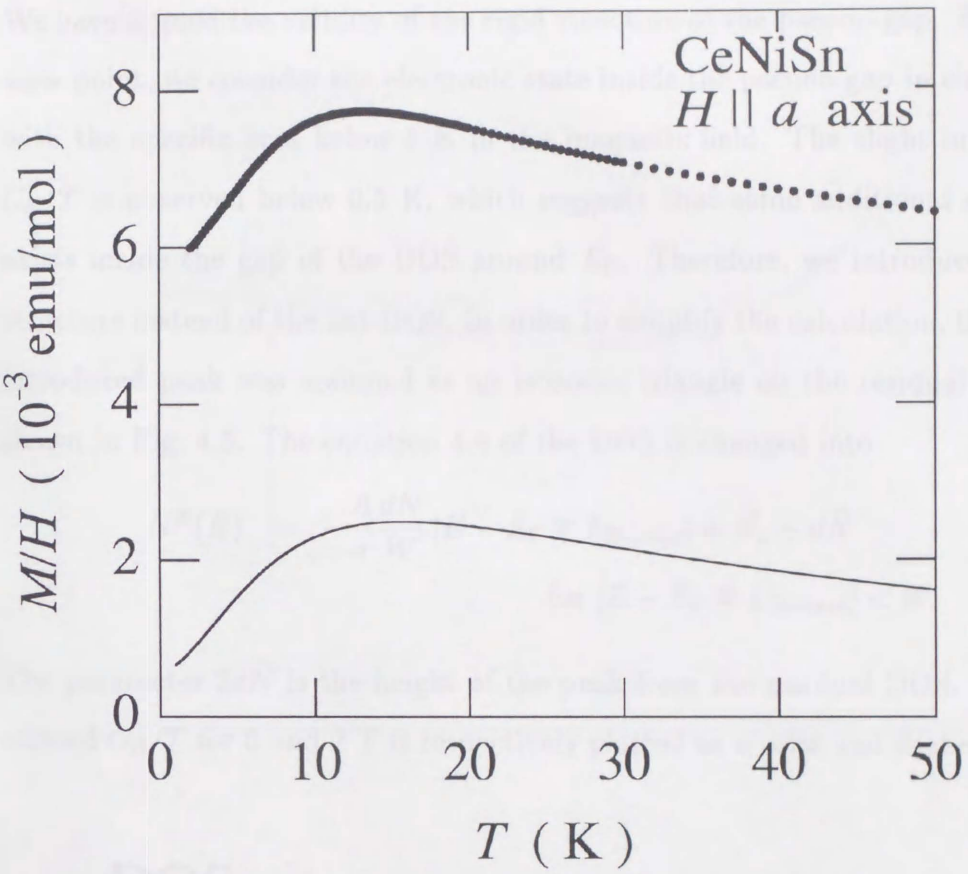

Figure 4.4: The calculated M/H for CeNiSn below 50 K. The closed circles are experimental data of M/H. The solid curve represents the χ_{cal} calculated by using the pseudo-gapped DOS model with the parameters shown in Fig. 4.2.

contribution. However, the magnitude of the difference, $\sim 5 \times 10^{-3}$ emu/mol, is much larger than the Van Vleck contribution to the magnetic susceptibility for the conventional metal. The difference may be explained by a Van-Vleck susceptibility enhanced by a many-body effect. Such an enhanced susceptibility is discussed in the cases of $Ce_3Bi_4Pt_3$ and YbB_{12} [43].

4.3 The electronic state inside the pseudo-gap

We have argued the validity of the rigid structure of the pseudo-gap. From this view point, we consider the electronic state inside the pseudo-gap in connection with the specific heat below 1 K in the magnetic field. The slight increase of C_{el}/T is observed below 0.5 K, which suggests that some additional structure exists inside the gap of the DOS around $E_{\rm F}$. Therefore, we introduce a peak structure instead of the flat DOS. In order to simplify the calculation, the newly introduced peak was assumed as an isosceles triangle on the residual DOS as shown in Fig. 4.5. The equation 4.4 of the DOS is changed into

$$N^{\pm}(E) = -\frac{A}{\pi}\frac{dN}{W}|E - E_{\rm F} \mp E_{\rm Zeeman}| + \widetilde{N}_0 + d\widetilde{N} \quad \text{for } |E - E_{\rm F} \mp E_{\rm Zeeman}| < W. \tag{4.7}$$

The parameter $2d\widetilde{N}$ is the height of the peak from the residual DOS. The calculated C_{el}/T for 0 and 2 T is respectively plotted as a solid and dashed curves

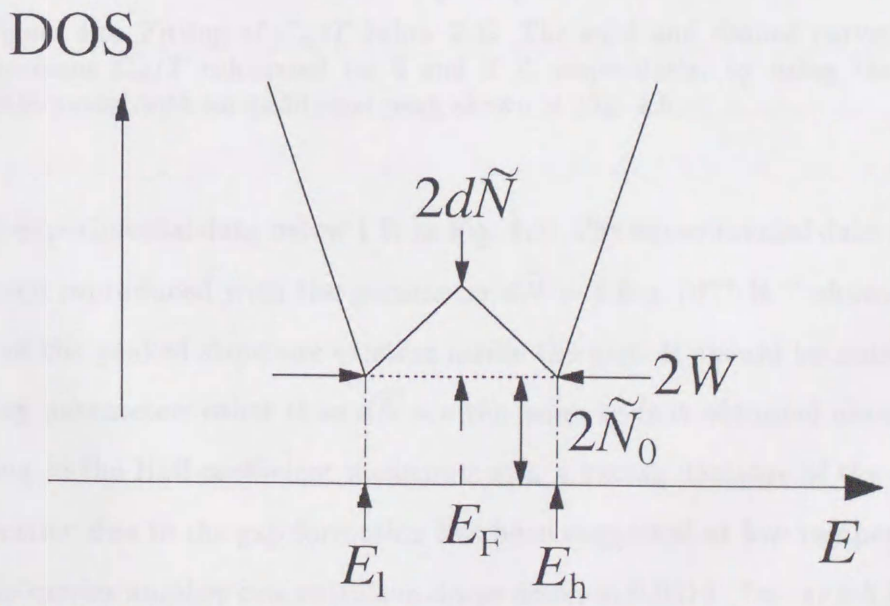

Figure 4.5: Additional peak structure at the bottom of the gap. The solid and dashed curves represent the peak structure and the flat residual DOS, respectively.

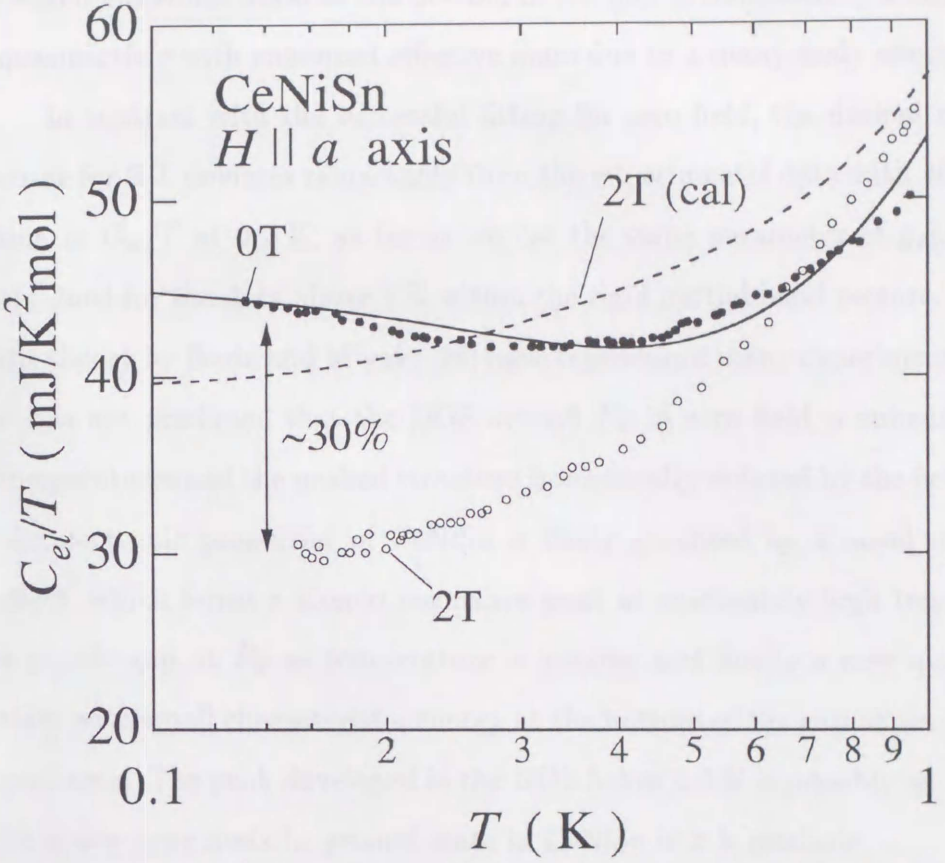

Figure 4.6: Fitting of C_{el}/T below 2 K. The solid and dashed curves represent C_{el}/T calculated for 0 and 2 T, respectively, by using the DOS model with an additional peak shown in Fig. 4.5.

with the experimental data below 1 K in Fig. 4.6. The experimental data at zero field is well reproduced with the parameter $d\widetilde{N} = 1.6 \times 10^{-4}$ K^{-1} showing the validity of the peaked structure existing inside the gap. It should be noted that the fitting parameters other than $d\widetilde{N}$ are the same as that obtained above 2 K. According to the Hall coefficient measurements, a strong decrease of the carrier concentration due to the gap formation has been suggested at low temperatures [39]. The carrier number concentration drops down to 0.0012 /f.u. at 0.5 K with an assumption of one carrier model. Concerning the values of C_{el}/T and the carrier concentration, we can roughly estimate the Sommerfeld coefficient γ per

one carrier at $\sim 10^4$ mol/K^{2}mol. The large value of γ strongly suggests that the peaked electronic state at the bottom of the gap is composed of a renormalized quasiparticle with enhanced effective mass due to a many-body effect.

In contrast with the successful fitting for zero field, the dashed calculation curve for 2 T deviates remarkably from the experimental data with 30 % reduction in C_{el}/T at 0.2 K, as far as we use the same parameter of $g_J|J_z| = 1.10$ obtained for the data above 2 K within the rigid partial band picture. Although the theory by Ikeda and Miyake [28] have reproduced many experimental results, it has not predicted that the DOS around E_F in zero field is enhanced at low temperatures and the peaked structure is drastically reduced by the field. Hence, the electronic properties of CeNiSn is likely governed by a novel many-body effect, which forms a Kondo resonance peak at moderately high temperatures, a pseudo-gap at E_F as temperature is lowered and finally a new quasiparticle state with small characteristic energy at the bottom of the gap at very low temperatures. The peak developed in the DOS below 0.5 K is possibly an indication for a new-type metallic ground state in CeNiSn if it is intrinsic.

Since C_{el}/T increases below 0.5 K in zero magnetic field, the electronic state should have a characteristic temperature $T^* \leq 1$ K, which corresponds to the Zeeman energy E_{Zeeman}/k_B for 1 T. It is quite reasonable that the new electronic state is dynamically collapsed by the magnetic field of ~ 1 T. Thus, the drastic reduction in C_{el}/T can be interpreted by the suppression of the new electronic state by the field. The increase of C_{el}/T above 2 T is reasonably explained by the overlap of the regions above E_h and below E_l in our DOS model (Fig. 4.1) due to the Zeeman effect. Because the additional peak structure in the DOS vanishes above 0.5 K, the initial decrease of C_{el}/T is not found in field dependence above 1 K. The T-linear dependence of C_{el}/T above 1 T suggests that the DOS is proportional to $|E_F - E|$ above 1 T.

In the above discussion, the new peak in the DOS has been treated as a new

intrinsic state of CeNiSn. We should examine a possibility of an extrinsic origin for the enhancement of C_{el}/T at low temperatures. One of the most possible candidates as the extrinsic origin is that an impurity band is responsible for the T and H dependence of C_{el}/T. However, the upturn of C_{el}/T below 0.5 K at zero field becomes clearer with purifying samples. This tendency suggests that the upturn is unlikely to result from impurities. The significant field effect below 4 T has been observed for the high-quality sample in this study. No appreciable field effect was seen for low quality samples in magnetic field along the a axis [23]. The impurity effect is expected to veil the field dependence of specific heat since the quasiparticle band is blurred out by the impurities. As mentioned above, C_{el}/T exhibits the strong anisotropy in respect to the direction of magnetic field. Isotropic or less anisotropic behavior against magnetic field is expected for impurities because the randomness introduced by the impurity makes the Fermi surface isotropic. Therefore, it is difficult to explain the strong anisotropy if one assume the impurity contribution. Thus, we believe that our findings are from intrinsic properties of the electronic ground state of CeNiSn.

Chapter 5

Conclusion

Measurements of thermal and magnetic properties for a high-quality single-crystalline CeNiSn in magnetic field allows us to investigate the intrinsic electronic ground state. Specific heat measurements have been performed from 0.1 to 25 K in magnetic field up to 14 T. A remarkable field effect is observed along the a axis in contrast with little field dependence for $H \parallel b$ and c. This anisotropy in specific heat is larger than that in magnetization.

The field dependence of the specific heat above 2 K is well explained by a V-shaped gap in the Lorentzian DOS with a residual DOS assuming the rigid band structure. The field effect is introduced only as the Zeeman splitting of the partial DOS for both up- and down-spin bands. We conclude from the result that the overall DOS as well as the pseudo-gap is hardly affected by the field in the temperature range above 2 K in magnetic field up to 14 T. The value $g_J|J_z| = 1.10$ obtained by fitting is close to the values of 1.29 expected for the CEF $|J = 5/2, J_z = \pm 3/2\rangle$ state, which supports the experimental and theoretical argument for the ground state of this compound.

The magnetic susceptibility has been measured from 2 to 600 K at the field of 1 T. Fitting the data to the Curie-Weiss formula yields the effective moment $\mu_{eff} = 2.53\mu_B$ and the paramagnetic Curie temperature $\theta_p = -42.6$ K. The value of $\mu_{eff} = 2.53\mu_B$ is close to the value $2.54\mu_B$ for the free Ce^{3+} ion. The rigid band picture can at least qualitatively reproduce the temperature dependence

of the magnetic susceptibility below 50 K. The cusp in M/H is found to arise from the presence of the pseudo-gapped DOS rather than from the enhancement of an antiferromagnetic correlation.

C_{el}/T slightly increases with lowering temperature below 0.5 K at zero field. The increase reveals that an additional peak structure exists at $E_{\rm F}$ inside the gap. The C_{el}/T enhanced below 0.5 K is reduced in turn by about 30 % as the field increases up to 2 T. The 30 % decrease is hardly explained by the rigid band picture.

The electronic properties of CeNiSn at low temperatures is concluded to be governed by a novel many-body effect, which forms a pseudo-gap in the Kondo resonance peak around $E_{\rm F}$. Below 0.5 K, the many-body interaction realizes a new quasiparticle state at the center of the gap. From this study, we propose that CeNiSn is a new type of strongly correlated metal although this compound has been so far classified as a Kondo insulator.

Acknowledgements

The author would like to express his sincere thanks to Professor Toshizo Fujita for his stimulating discussion and encouragement through the course of this study. He is also grateful to Associate Professor Takashi Suzuki for fruitful discussion and useful advice. He would like to thank Professor Toshiro Takabatake, Professor Hironobu Fujii, Professor Kunihiko Maezawa and Dr. Go Nakamoto for the preparation of a high-quality single-crystalline CeNiSn and valuable discussion. He wishes to express his appreciation to Associate Professor Yoshiteru Maeno for helpful discussion and Professor Kazumasa Miyake for precious advice of theoretical aspects for CeNiSn. He gratefully acknowledge helpful discussions with attendance at collaboration meeting on "Coherence and Spin Correlations in Kondo Semiconductors" in Switzerland on several points in this study. He also thanks to Mitsue Kitamura, Yasuyoshi Matsumoto and other colleagues of Fujita Laboratory for their technical supports. He is indebted to the cryogenic center for supplying the liquid helium and to the technical workshop of the faculty of science for making the parts of equipments for this study. Finally, I would like to thank my parents and my friends for their warmhearted helps.

Bibliography

[1] K. Andres, J. E. Craebner, and H. R. Ott, Phys. Rev. Lett. **35**, 1779 (1975).

[2] G. R. Stewart, Rev. Mod. Phys. **56**, 755 (1984).

[3] N. Grewe and F. Steglich, in *Handbook on the physics and Chemistry of Rare Earths, Vol. 14*, edited by J. K. A. Gschneidner and L.Eyring (Elservier Science Publishers B.V., Amsterdam, 1991), p. 343.

[4] T. Fujita, T. Suzuki, S. Nishigori, T. Takabatake, H. Fujii, and J. Sakurai, J. Magn. Magn. Mater. **108**, 35 (1992).

[5] T. Takabatake, F. Teshima, H. Fujii, S. Nishigori, T. Suzuki, T. Fujita, Y. Yamaguchi, and J. Sakurai, Phys. Rev. B **41**, 9607 (1990).

[6] M. Kyogaku, Y. Kitaoka, H. Nakamura, K. Asayama, T. Takabatake, F. Teshima, and H. Fujii, J. Phys. Soc. Jpn. **59**, 1728 (1990).

[7] S. Nishigori, H. Goshima, T. Suzuki, T. Fujita, G. Nakamoto, H. Tanaka, T. Takabatake, and H. Fujii, J. Phys, Soc. Jpn. **65**, 2614 (1996).

[8] T. Ekino, T. Takabatake, H. Tanaka, and H. Fujii, Phys. Rev. Lett. **75**, 4262 (1995).

[9] M. F. Hundley, P. C. Canfield, J. D. Thompson, and Z. Fisk, Phys. Rev. B **42**, 6842 (1990).

[10] S. K. Malik and D. T. Adroja, Phys. Rev. B **43**, 6277 (1991).

[11] J. W. Allen, R. M. Martin, B. Batlogg, and P. Wachter, J. Appl. Phys. **49**, 2078 (1978).

[12] M. Kasaya, F. Iga, K. Negishi, S. Nakai, and T. Kasuya, J. Magn. Magn. Mater. **31-34**, 437 (1983).

[13] R. V. Skolozdra, O. E. Koretskaya, and Y. K. Gorelenko, Inorg. Mater. **20**, 604 (1984).

[14] I. Higashi, K. Kobayashi, T. Takabatake, and M. Kawaya, J. Alloys and Compounds **193**, 300 (1993).

[15] T. E. Mason, G. Aeppli, A. P. Ramirez, K. N. Clausen, C. Broholm, N. Stücheli, E. Bucher, and T. T. M. Palstra, Phys. Rev. Lett. **69**, 490 (1992).

[16] M. Kohgi, K. Ohoyama, T. Osakabe, M. Kasaya, T. Takabatake, and H. Fujii, Physica B **186-188**, 409 (1993).

[17] D. T. Adroja, B. D. Rainford, A. J. Neville, and A. G. M. Jansen, Physica B **223-224**, 275 (1996).

[18] T. Takabatake, M. Nagasawa, H. Fujii, G. Kido, K. Sugiyama, K. Senda, K. Kido, and M. Date, Physica B **172**, 177 (1992).

[19] S. Holtmeier, C. Hinkel, M. Aigner, G. Bruls, D. Finsterbusch, B. Wolf, W. Assmus, and B. Lüthi, Physica B **230-232**, 658 (1997).

[20] M. Kasaya, F. Iga, M. Takigawa, and T. kasuya, J. Magn. Magn. Mater. **47-48**, 429 (1985).

[21] A. P. Reys, R. H. Heffner, P. C. Canfield, J. D. Thompson, and Z. Fisk, Phys. Rev. B **49**, 16321 (1994).

[22] K. Nakamura, Y. Kitaoka, K. Asayama, T. Takabatake, G. Nakamoto, H. Tanaka, and H. Fujii, Physica B **206-207**, 829 (1995).

[23] T. Takabatake, M. Nagasawa, H. Fujii, G. Kido, M. Nohara, S. Nishigori, T. Suzuki, T. Fujita, R. Helfrish, U. Ahlheim, K. Fraas, C. Geibel, and F. Steglich, Phys. Rev. B **45**, 5740 (1992).

[24] T. Nishino and K. Ueda, Phys. Rev. B **47**, 12451 (1993).

[25] T. Kasuya, J. Phys. Soc. Jpn. **65**, 2548 (1996).

[26] T. Mutou and D. S. Hirashima, J. Phys. Soc. Jpn. **63**, 4475 (1994).

[27] Y. Kagan, K. A. Kikoin, and A. S. Mishchenko, Phys. Rev. B **55**, 12348 (1997).

[28] H. Ikeda and K. Miyake, J. Phys. Soc. Jpn. **65**, 1769 (1996).

[29] G. Nakamoto, T. Takabatake, H. Fujii, A. Minami, K. Maezawa, I. Oguro, and A. A. Menovsky, J. Phys. Soc. Jpn. **64**, 4834 (1995).

[30] G. Nakamoto, T. Takabatake, Y. Bando, H. Fujii, K. Izawa, T. Suzuki, T. Fujita, A. Minami, I. Oguro, L. T. Tai, and A. A. Menovsky, Physica B **206-207**, 840 (1995).

[31] T. Takabatake, G. Nakamoto, T. Yoshino, H. Fujii, K. Izawa, S. Nishigori, H. Goshima, T. Suzuki, T. Fujita, K. Maezawa, T. Hiraoka, Y. Okayama, I. Oguro, A. A. Menovsky, K. Neumaier, A. Brückl, and K. Andres, Physica B **223-224**, 413 (1996).

[32] F. Iga, N. Shimizu, and T. Takabatake, to appear in J. Magn. Magn. Mater. (1998).

[33] J. C. Cooley, M. C. Aronson, and P. C. Canfield, Phys. Rev. B **55**, 7533 (1997).

[34] T. Fujita, M. Suzuki, T. Komatsubara, S. Kunii, T. Kasuya, and T. Ohtsuka, Solid State Commun. **35**, 569 (1980).

[35] H. v. Löhneysen, T. Pietrus, G. P. H. G. Schlager, A. Schröder, M. Sieck, and T. Trappmann, Phys. Rev. Lett. **72**, 3262 (1994).

[36] H. Amitsuka, T. Hidano, T. Honma, H. Mitamura, and T. Sakakibara, Physica B **186-188**, 337 (1993).

[37] D. Jaccard, K. Behnia, and J. Sierro, Phys. Lett.A **163**, 475 (1992).

[38] K. Andres and T. Takabatake, private communications .

[39] T. Takabatake, F. Iga, T. Yoshino, Y. Echizen, K. Kobayashi, M. Higa, K. Katoh, N. Shimizu, Y. Bando, G. Nakamoto, H. Fujii, K. Izawa, T. Suzuki, T. Fujita, M. Sera, M. Hiroi, K. Maezawa, S. Mock, H. v. Löneysen, A. Brückl, K. Neumaier, and K. Andres, to appear in J. Magn. Magn. Mater. (1998).

[40] T. Suzuki, H. Fujisaki, T. Fujita, G. Nakamoto, T. Takabatake, H. Fujii, and A. Tamaki, J. Magn. Magn. Mater. **140-144**, 1215 (1995).

[41] T. Saso, J. Phys. Soc. Jpn. **66**, 1175 (1997).

[42] T. Saso, private communications .

[43] H. Kontani and K. Yamada, J. Phys. Soc. Jpn. **65**, 172 (1996).

公表論文

(1) The Origin of Magnetic Field Dependence of Specific Heat in Single-Crystalline CeNiSn

K. Izawa, T. Suzuki, M. Kitamura, T. Fujita,T. Takabatake, G. Nakamoto, H. Fujii and K. Maezawa

Journal of the Physical Society of Japan **65** (10), 3119-3122 (1996).

(2) Anomalous field dependence of specific heat of CeNiSn below 1K

K. Izawa, T. Suzuki, T. Fujita, T. Takabatake, G. Nakamoto, H. Fujii and K. Maezawa

Journal of Magnetism and Magnetic Materials **177-181**, 395-396 (1998).

参考論文

(1) Different Electronic Ground States in the Hexagonal and Cubic Phases of UAu_2Sn

K. Izawa, T. Suzuki, T. Fujita, Y. Maeda, T. Takabatake and H. Fujii

Journal of the Physical Society of Japan **65** (10), 3260-3265 (1996).

(2) Effect of high magnetic field on gap formation in CeNiSn

K. Izawa, T. Suzuki, M. Kitamura, T. Fujita, G. Nakamoto, T. Takabatake and H. Fujii

Physica B **230-232**, 670-672 (1997).

(3) Polymorphism and heavy-fermion behavior in UAu_2Sn

Y. Maeda, T. Takabatake, H. Fujii, K. Izawa, T. Suzuki, T. Fujita, A. Minami, K. Oda, K. Sugiyama and K. Kindo

Journal of Magnetism and Magnetic Materials **140-144**, 1363-1364 (1995).